

# Aneuploidy can be an evolutionary detour on the path to adaptation

Ilia Kohanovski<sup>a,b,\*</sup>, Martin Pontz<sup>a,\*</sup>, Orna Dahan<sup>c</sup>, Yitzhak Pilpel<sup>c</sup>, Avihu H.  
Yona<sup>d</sup>, and Yoav Ram<sup>a,1</sup>

<sup>a</sup>School of Zoology, Faculty of Life Sciences, Tel Aviv University, Tel Aviv, Israel

<sup>b</sup>School of Computer Science, Reichman University, Herzliya, Israel

<sup>c</sup>Department of Molecular Genetics, Weizmann Institute of Science, Rehovot, Israel

<sup>d</sup>Institute of Biochemistry, Food Science and Nutrition, Robert H. Smith Faculty of Agriculture, Food and Environment, The Hebrew University of Jerusalem, Israel

\*These authors contributed equally to this work

<sup>1</sup>Corresponding author: yoav@yoavram.com

November 24, 2022

Classifications. Biological Sciences: Evolution, Genetics, Microbiology, Population Biology.

Keywords: whole-chromosome duplication, evolutionary model, adaptive evolution

## Abstract

16 Aneuploidy is common in eukaryotes, often leading to decreased growth and fitness. How-  
18 ever, evidence from yeast and other fungi, as well as human tumour cells, suggests that specific  
20 aneuploidies can be beneficial under stressful conditions and facilitate adaptation. In a prominent  
22 example, an evolutionary experiment with yeast, populations evolving under heat stress had be-  
come aneuploid (chromosome III), only to later revert back to euploid after genetic mutations have  
accumulated. It has therefore been suggested that aneuploidy serves as a "stepping stone" on the  
path to adaptation.

24 Here, we test this hypothesis. First, we apply DNA sequencing to show that mutant alleles  
common in aneuploid cells are uncommon in the evolved euploid population. Second, we develop  
26 an evolutionary model with both aneuploidy and mutation, and fit it to the results of the experiment  
using a Bayesian inference framework. We then predict the genotype frequency dynamics during  
the experiment, demonstrating that the majority of the evolved euploid population likely did not  
28 descend from aneuploid cells, but rather directly from the euploid wild-type population. Our  
model shows how the beneficial mutation supply—the product of population size and beneficial  
30 mutation rate—determine the evolutionary dynamics: with a low mutation supply, a large fraction  
of the evolved population may descend from aneuploid cells; but with a high mutation supply,  
32 beneficial mutations are generated before fixation of aneuploidy, and can outcompete aneuploidy  
due to the latter's inherent fitness cost.

34 Together, our results suggest that aneuploidy can be an evolutionary "detour" rather than a  
"stepping stone": it can delay, rather than facilitate, the adaptation of the population, and cells that  
36 become aneuploid may leave less descendants compared to cells that remain diploid.

# Introduction

38 Aneuploidy is an imbalance in the number of chromosomes in the cell: an incorrect karyotype.  
Evidence suggests aneuploidy is very common in eukaryotes, e.g. animals<sup>42,33,2</sup>, and fungi<sup>36,65,40,54</sup>.  
40 Aneuploidy has been implicated in cancer formation, progression, and drug resistance<sup>4,44,42,21</sup>. It  
is also common in protozoan pathogens of the *Leishmania* genus, a major global health concern<sup>31</sup>,  
42 and contributes to the emergence of drug resistance<sup>45</sup> and virulence<sup>32</sup> in fungal pathogens, which  
are under-studied<sup>41</sup>, despite infecting a billion people per year, causing significant morbidity in >150  
44 million and death in >1.5 million people per year<sup>45,41</sup>.

Experiments with human and mouse embryos found that most germline aneuploidies are lethal. An-  
46 euploidies are also associated with developmental defects and lethality in other multicellular organ-  
isms<sup>48</sup>. For example, aneuploid mouse embryonic cells grow slower than euploid cells<sup>59</sup>. Similarly,  
48 in unicellular eukaryotes growing in benign conditions, aneuploidy usually leads to slower growth and  
decreased overall fitness, in part due to proteotoxic stress due to increased expression, gene dosage  
50 imbalance, and hypo-osmotic-like stress<sup>34,57,36,48,43,24,64,58,60</sup>.

However, aneuploidy can be beneficial under stressful conditions due to the wide range of phenotypes  
52 it can produce, some of which are advantageous<sup>36,60</sup>. Indeed, in a survey of 1,011 yeast strains,  
aneuploidy has been detected in about 19%<sup>37</sup>. Thus, aneuploidy can lead to rapid adaptation in  
54 unicellular eukaryotes<sup>15,56,19,39</sup>, as well as to rapid growth of somatic tumour cells<sup>44,50</sup>. For example,  
aneuploidy in *Saccharomyces cerevisiae* facilitates adaptation to a variety of stressful conditions  
56 like heat and pH<sup>62</sup>, copper<sup>7,15</sup>, salt<sup>10</sup>, and nutrient limitation<sup>11,17,1</sup>, with similar results in *Candida*  
*albicans*<sup>60</sup>. Importantly, aneuploidy can also lead to drug resistance in pathogenic fungi such as  
58 *C. albicans*<sup>47,46,14</sup> and *Cryptococcus neoformans*<sup>51</sup>, which cause candidiasis and meningoencephalitis,  
respectively.

60 Yona et al.<sup>62</sup> demonstrated experimentally the importance of aneuploidy in adaptive evolution. They  
evolved populations of *S. cerevisiae* under strong heat stress. The populations adapted to the heat stress  
62 within 450 generations, and this adaptation was determined to be due a duplication of chromosome III.  
Later on, after more than 1,500 generations, the populations reverted back to an euploid state, while  
64 remaining adapted to the heat stress. Aneuploidy was therefore suggested to be a *transient adaptive*  
*solution*, because it can rapidly appear and fixate in the population under stressful conditions, and can  
66 then be rapidly lost when the cost of aneuploidy outweighs its benefit—after the stress is removed,  
or after "refined" beneficial mutations appear and fixate<sup>62</sup>. Furthermore, it has been suggested that  
68 aneuploidy is an evolutionary "stepping stone" that facilitates future adaptation by genetic mutations,

which require more time to evolve<sup>62,61</sup>.

70 Here, we test the hypothesis that aneuploidy is a *an evolutionary stepping stone* that facilitates adaptive evolution by genetic mutations Yona et al.<sup>61</sup>. First, we sequenced the genomes of evolved populations  
72 reported in<sup>62</sup> and analyzed their mutant allele frequencies to assess if the evolved euploid cells are descended from aneuploid cells. Second, we develop an evolutionary genetic model and fit it to  
74 the experimental results of Yona et al.<sup>62</sup> in order to predict the genotype frequency dynamics in the experimental populations, thereby estimating the frequency of evolved euploid cells that descended  
76 from aneuploid cells. Our results show that aneuploidy reached high frequencies in the experimental populations, but nevertheless, the majority of cells in the evolved euploid population likely did not  
78 descend from aneuploid cells, but rather directly from wild-type euploid cells. These results suggest that at the lineage level, aneuploidy may be an evolutionary detour, rather than a stepping stone, on  
80 the path to adaptation.

## Results

82 In the heat-stress experiment of Yona et al.<sup>62</sup>, four populations of *S. cerevisiae* evolved under 39 °C.  
Aneuploidy fixed in all four experimental repetitions in the first 450 generations. Two of the repetitions,  
84 marked *H2* and *H4*, carried no large-scale duplications other than a chromosome III trisomy. These two repetitions continued to evolve under the same conditions, wherein aneuploidy was eliminated by  
86 generation 1,700 and 2,350 in *H4* and *H2*, respectively.

**Empirical frequencies of mutant alleles.** For each of two evolved populations (*H2* and *H4*) we  
88 sequenced the ancestral diploid population (generation 0), the aneuploid population (generation 450), and the evolved euploid population (generation 1,700 or 2,350) to estimate the mutant allele frequencies  
90 (Tables S1 and S2). Overall, between 100 and 173 mutant alleles were detected with at least a single read in the six populations that were sampled. Disregarding 45 and 40 alleles that were present in  
92 the ancestral populations at a frequency >10%, the aneuploid and euploid populations carried a large number of mutant alleles: 82 and 95, respectively, in repetition *H2*, and 60 and 66 in repetition  
94 *H4*.

Surprisingly, out of all these mutant alleles, none was present at a frequency >20% in both the  
96 aneuploid and the evolved euploid populations. More importantly, a high mutant allele frequency in the aneuploid population was associated with a low frequency in the evolved euploid population,  
98 and vice-versa (Spearman's correlation coefficient  $\rho = -0.64$  and  $-0.66$  in the two experimental

repetitions; Figure 1), suggesting that mutant alleles frequent in the aneuploid populations decreased 100 in frequency when aneuploidy was lost. These results suggest evolved euploid cells are unlikely to have descended from aneuploid cells.

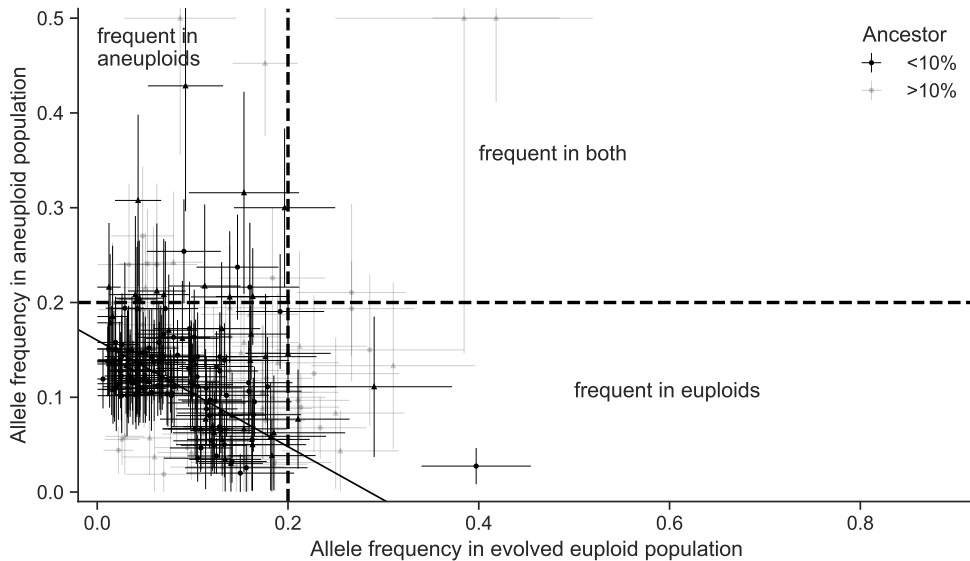


**Figure 1: Frequencies of mutant alleles in the experimental populations are negatively correlated.** Frequencies of mutant alleles when trisomy was widespread in the population (y-axis) and after it was eliminated (x-axis) in two experimental repetitions (circles for *H2* and triangles for *H4*) from Yona et al.<sup>62</sup>. Mutant alleles with >20% in the aneuploid population were <20% in the euploid population, and vice versa (the upper-right quadrant is empty), suggesting that the majority of evolved euploid cells did not descend from the most common aneuploid genotypes. Alleles with frequency below and above 10% in the ancestral populations are in black and gray, respectively. Solid black line is a linear orthogonal distance regression line (slope=−0.559, intercept=0.164; a regression through alleles that reach at least 20% in one of the populations has slope=−0.645 and intercept=0.297). Dashed vertical and horizontal lines show allele frequencies of 20%. Error bars show SEM (standard error of the mean) assuming the number of reads in Binomially distributed; the SEM may be large when the total number of reads is small. For the 18 mutant alleles with high frequency in the aneuploid populations (>20%), the highest frequencies in the euploid populations were 15.4%, 16%, 16.3% and 19.6% (the rest were below 15%). Similarly, for the 48 mutant alleles with high frequency in the evolved euploid populations, the highest frequencies in the aneuploid populations were 2.7%, 7.7%, and 11.1% (the rest were below 1%).

102 **Evolutionary genetic model.** To explore the dynamics during the evolutionary experiments, we developed an evolutionary genetic model, fitted the model to empirical data, and used it to predict the 104 genotype frequency dynamics, or specifically, the fraction of the evolved euploid population descended

from aneuploid cells.

106 The model includes the effects of natural selection, genetic drift, aneuploidy, and mutation, and follows  
108 a population of cells characterized by their genotype: euploid wild-type,  $2n$ , is the ancestral diploid  
110 genotype; euploid mutant,  $2n^*$ , has a diploid karyotype and a single beneficial mutation; aneuploid  
112 wild-type,  $2n+1$ , has an extra chromosome due to a chromosome duplication event; and aneuploid  
mutant,  $2n+1^*$ , has an extra chromosome (like  $2n+1$ ) and a beneficial mutation (like  $2n^*$ ). Fitness  
values of the different genotypes are denoted by  $w_{2n}$ ,  $w_{2n^*}$ ,  $w_{2n+1}$ , and  $w_{2n+1^*}$ , and the rate of mutation  
and aneuploidy are denoted by  $\mu$  and  $\delta$ , respectively. See Figure 2 for an illustration of the model.

We fitted this model to the experimental results<sup>62</sup> – time for fixation (>95%) and for loss (<5%) of  
114 aneuploidy – using approximate Bayesian computation with sequential Monte Carlo (ABC-SMC)<sup>52</sup>,  
thereby inferring the model parameters: rates aneuploidy and mutation and the fitness of all genotypes.  
116 We then sampled posterior predictions for the genotype frequency dynamics using the estimated  
parameter values and compared different versions of the model to test additional hypotheses about the  
118 evolutionary process.

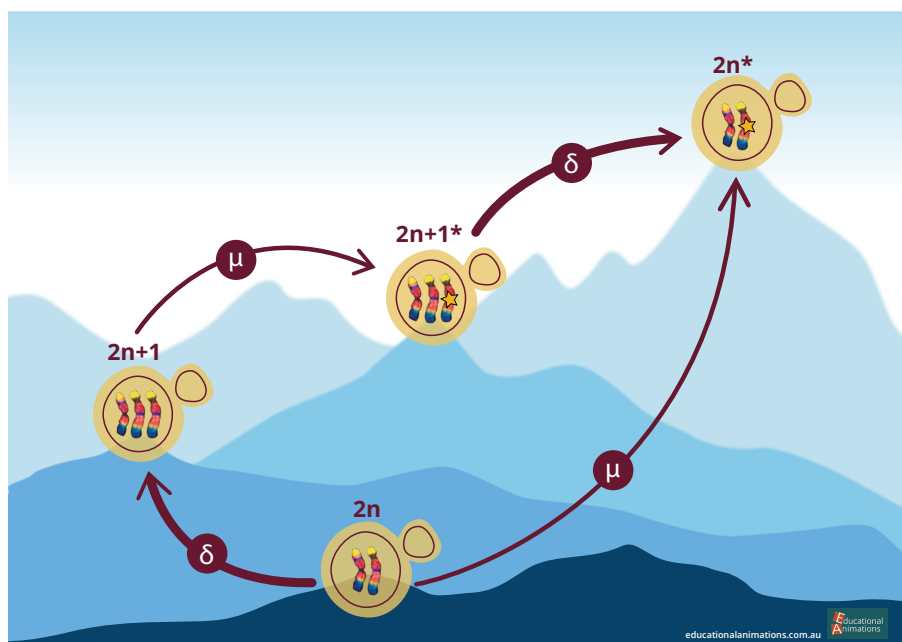


**Figure 2: Model Illustration.** There are four genotypes in our model: euploid wild-type,  $2n$ ; euploid mutant,  $2n^*$ ; aneuploid wild-type,  $2n+1$ ; and aneuploid mutant,  $2n+1^*$ . Overall there are two possible trajectories from  $2n$  to  $2n^*$ . Arrows denote transitions between genotypes, with transition rates  $\mu$  for the beneficial mutation rate and  $\delta$  for the aneuploidy rate. Elevation differences illustrate the expected, rather than the assumed, fitness differences between the genotypes.

**Estimated rates and fitness effects of aneuploidy and mutation.** We inferred the posterior distribution of model parameters (Figure 3). We report parameter estimates using the MAP (maximum a

120 posteriori) and providing the 50% HDI (highest density interval) in square brackets. See Supplementary Material for sensitivity analysis.

The estimated beneficial mutation rate is  $\mu = 2.965 \cdot 10^{-6}$  [ $2.718 \cdot 10^{-7} - 3.589 \cdot 10^{-6}$ ]. From the literature, the mutation rate per base pair is roughly  $2 - 3 \cdot 10^{-10}$  (refs.<sup>66,30</sup>), but it may be higher under heat stress, as several stresses<sup>18</sup>, including heat<sup>20</sup>, may cause hypermutation in yeast. If we assume a 10-fold increase over the mutation rate reported in the literature, then the estimated beneficial mutation rate can be explained by a genomic target size of 1,000 base pairs (i.e., 1,000 base pairs across the genome in which a mutation would provide a fitness benefit). Supporting this, Flynn et al.<sup>12</sup> used a deep mutational scan of a single protein, Hsp90, to find 465 amino-acid variants that increased growth rate in 37 °C. Furthermore, Yona et al.<sup>62</sup> found at least 10 genes on chromosome III that increased heat tolerance when over-expressed. Assuming that other chromosomes also have a similar number of heat-tolerance genes (and even more, as chromosome III is one of the smallest chromosomes<sup>16</sup>), we get a total of 160 heat-tolerance genes in the genome. Indeed, mutations were found in 97 genes in an evolutionary experiment with yeast under heat stress<sup>20</sup>. Thus, to get a genomic target size of 1,000, it is enough that the average gene target size is 6.25 base pairs. For example, Kohn and Anderson<sup>27</sup> found a target size of 11 in a proton exporter gene (*PMA1*) that contributes to high-salt adaptation.

The estimated aneuploidy rate,  $\delta = 1.72 \cdot 10^{-3}$  [ $1.47 \cdot 10^{-3} - 2.786 \cdot 10^{-3}$ ] is higher than in previous studies: for chromosome III in diploid *S. cerevisiae*, Zhu et al.<sup>66</sup> estimated  $6.7 \cdot 10^{-6}$  chromosome gain events per generation, and Kumaran et al.<sup>29</sup> estimate  $3.0 \cdot 10^{-5} - 4.3 \cdot 10^{-5}$  chromosome loss events per generation (95% confidence interval). However, this difference may be partly explained by an increased aneuploidy rate during heat stress: heat shock can increase the rate of chromosome fragment loss by 2-3 orders of magnitude<sup>5</sup>.

The estimated fitness values are  $w_{2n+1} = 1.022$  [ $1.021 - 1.023$ ],  $w_{2n+1*} = 1.025$  [ $1.024 - 1.026$ ],  $w_{2n*} = 1.028$  [ $1.026 - 1.029$ ], all relative to the fitness of  $2n$ , which is set to  $w_{2n} = 1$ . Thus, we can infer that the cost of chromosome III trisomy is  $c = w_{2n*} - w_{2n+1*} = 0.003$  (or 0.3%) and the benefit of trisomy is  $w_{2n+1} - 1 - c = 0.019$  (1.9%), whereas the benefit of the beneficial mutation is  $w_{2n*} - 1 = 0.028$  (2.8%).

If we allow for transitions (mutation, chromosome loss and gain) to less-fit genotypes (e.g.,  $2n^*$  to  $2n+1^*$ ), then we infer similar but slightly different values, see Supplementary Material.

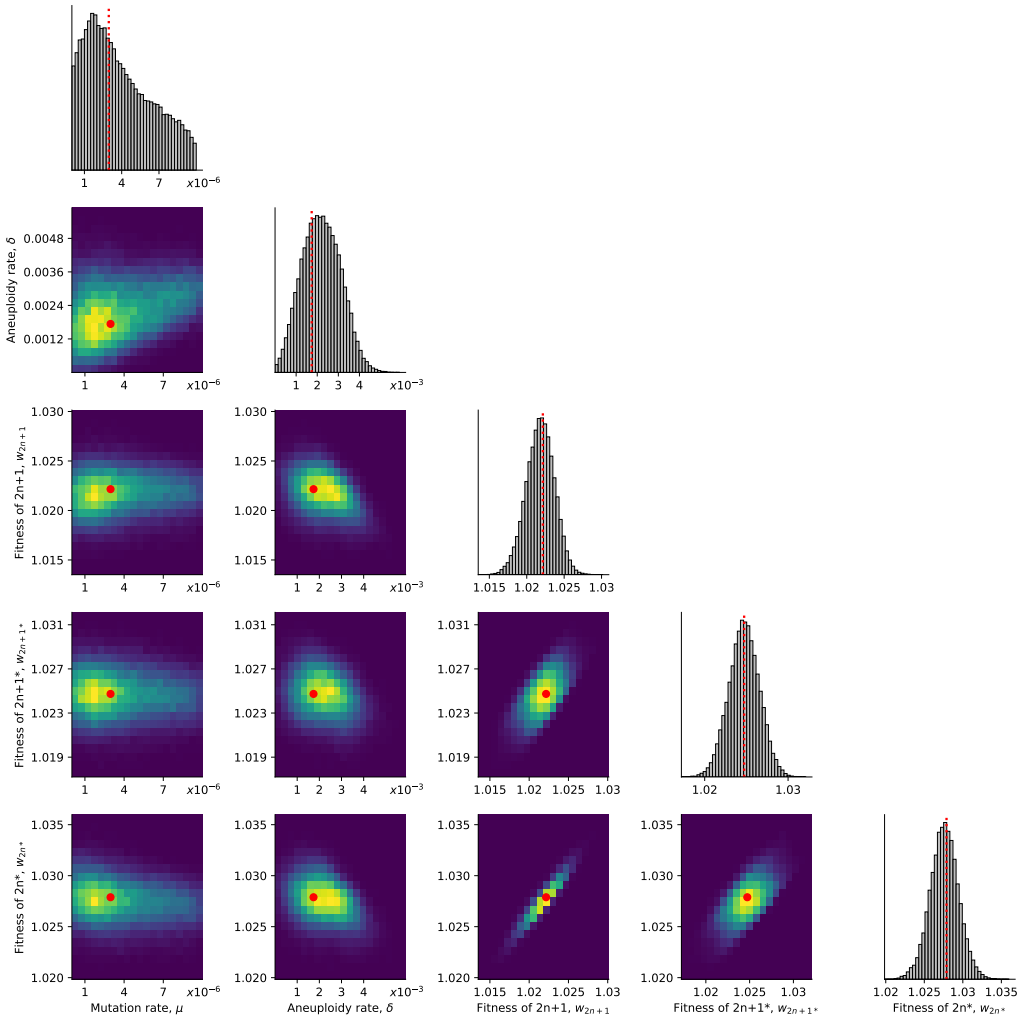


**Figure 3: Posterior distribution of model parameters.** On the diagonal, the marginal posterior distribution of each model parameter. Below the diagonal, the joint posterior distribution of pairs of model parameters (dark purple and bright yellow for low and high density, respectively). Red markers and orange lines for the joint MAP estimate (which may differ from the marginal MAP, as the marginal distribution integrates over all other parameters).

150 **Model comparison and goodness-of-fit.** To assess the fit of our model to the data, we use posterior  
151 predictive checks, in which we simulate the frequency dynamics using MAP parameter estimates and  
152 compare them to the data. Our model fits the data well:  $2n^*$  fixed in 61% of simulations by generation  
1,700 and in 100% of simulations by generation 2,350 (Figure 4).

154 However, a model without aneuploidy (where the aneuploidy rate is fixed at zero,  $\delta = 0$ ), fails to  
155 explain the experimental observations (Figure 4). The estimated mutation rate without aneuploidy is  
156  $\mu = 7.98 \cdot 10^{-9}$  [ $7.906 \cdot 10^{-9} - 8.138 \cdot 10^{-9}$ ], much lower compared to a model with aneuploidy. The  
157 fitness of the mutant is also much lower at  $w_{2n^*} = 1.013$  [ $1.012 - 1.013$ ]. This is because, without  
158 aneuploidy, a high mutation rate or fitness effect will lead to faster appearance and fixation of  $2n^*$  than

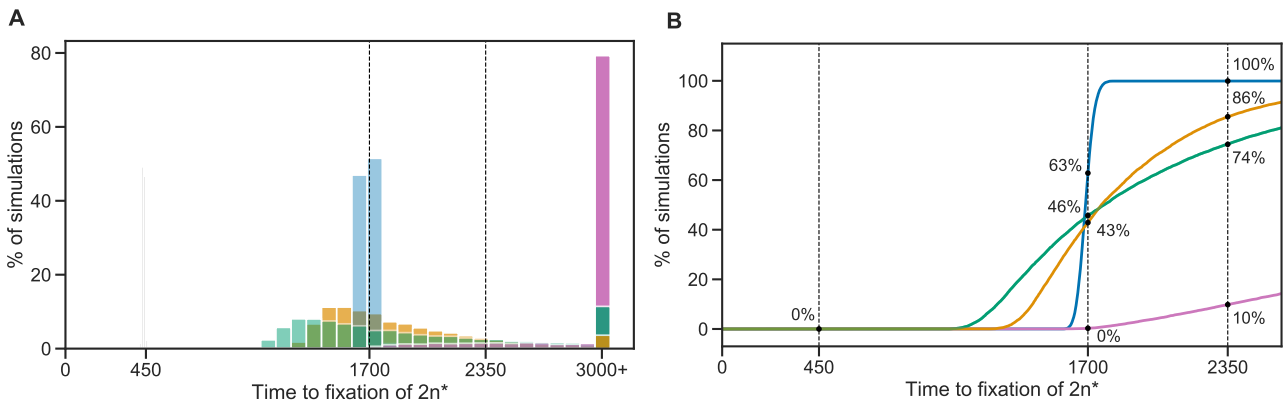


**Figure 4: Model fit with and without aneuploidy.** The distribution of time to fixation of  $2n^*$  (i.e., adaptation time) in 10,000 simulations using MAP parameters of the model with beneficial aneuploidy (blue;  $\delta > 0$ ,  $w_{2n} < w_{2n+1} < w_{2n+1^*} < w_{2n^*}$ ) compared to alternative models: a model with the same parameter values but without aneuploidy (gray,  $\delta = 0$ , concentrated at  $t = 450$ ); a model fitted to the data assuming no aneuploidy (green,  $\delta = 0$ ); a model fitted to the data assuming neutral aneuploidy (yellow,  $\delta > 0$ ,  $w_{2n+1} = w_{2n}$ ,  $w_{2n+1^*} = w_{2n^*}$ ); and a model with beneficial aneuploidy and an extended prior distribution (pink). In the experiment by Yona et al.<sup>62</sup>, one population lost aneuploidy by generation 1,700 and another by generation 2,350 (dashed lines) but not before generation 450. Thus, the blue distribution has a better fit compared to the other distributions (the gray distribution has a particularly poor fit). The MAP likelihood (eq. (4)) is 0.84, 0.78, 0.67, and 0.14 for the models represented by blue, yellow, green, and pink distributions, respectively. **(A)** Histogram of the time to fixation of  $2n^*$ . The last bin contains all values equal or greater than 3,000. **(B)** Cumulative distribution of the time to fixation.

in the experimental observations.

160 We also checked a model in which aneuploidy occurs but is adaptively neutral compared to the wild-type, that is,  $w_{2n+1} = w_{2n}$  and  $w_{2n+1^*} = w_{2n^*}$  but  $\delta > 0$ . This model fits the data better than the model  
 162 with no aneuploidy (in which  $\delta = 0$ ), but worse than a model with positive selection for aneuploidy, in which  $w_{2n} < w_{2n+1} < w_{2n+1^*} < w_{2n^*}$  (Figure 4).

164 **Model predictions of genotype frequency dynamics.** We simulated 50 replicate genotype frequency dynamics using the MAP estimate parameters. Figure 5A shows the simulated frequencies of  
 166 the four genotypes ( $2n$ ,  $2n+1$ ,  $2n+1^*$  and  $2n^*$ ), as well as the frequencies of  $2n^*$  cells that arose from either  $2n+1$  cells via a sequences of mutation and chromosome loss events ( $2n_A^*$ ), or directly from  
 168  $2n$  cells via a mutation event ( $2n_M^*$ ). We find that  $2n+1^*$  never reaches substantial frequency as it is quickly replaced by  $2n^*$  in a process similar to *stochastic tunneling*<sup>22,28</sup>.

170 To test the hypothesis that aneuploidy facilitates adaptation, we estimated  $F_A$ , the expected frequency  
of  $2n^*$  that arose from  $2n+1$ , computed as the average frequency of such  $2n_A^*$  cells at the end of  
172 simulations using the MAP estimate parameters. Surprisingly, we observe that the majority of  $2n^*$   
cells are  $2n_M^*$ , a product of a direct mutation in  $2n$  cells, rather than descending from  $2n+1$  cells  
174 ( $F_A^{MAP} = 0.106$ , average end point of 50 purple lines in Figure 5A). This is despite the fact that the  
 $2n+1$  genotype reaches high frequencies in the population (at least 0.98, Figure 5A).

176 This result is not unique to the MAP parameter estimate. We simulated genotype frequency dynamics  
using parameter samples from the posterior distribution, and computed the posterior distribution of  $F_A$   
178 (Figure 5B). The posterior mode  $F_A$  was just 0.147 [0.0154-0.370 95% CI] and only in 489 of 100,000  
posterior samples (0.489%)  $F_A$  was larger than 0.5 (see Supporting Material for results when transitions  
180 to less-fit genotypes are allowed, such as  $2n^*$  to  $2n+1^*$ ). Thus, if we sample a random cell from the  
evolved  $2n^*$  population, it is more likely to have descended directly from an euploid cell than from  
182 an aneuploid cell. The probability of  $2n^*$  descending from  $2n+1$  ( $F_A$ ) increases with the aneuploidy  
rate,  $\delta$ , and decreases with both the population size  $N$  and the mutation rate,  $\mu$  (Figure 5C,D). In some  
184 cases it can also be affected by the fitness parameters (Figure S10).

**Genetic instability in aneuploid cells.** It has been suggested that aneuploidy increases genetic  
186 instability<sup>49,21</sup>. Therefore, we inferred model parameters under the assumption that the mutation rate  
increases in aneuploid cells by a factor  $\tau = 1, 33/32$  (due to an additional chromosome), 2, 5, 10, or  
188 100 (due to genetic instability). We found that the posterior distribution was similar for  $\tau = 1, 33/32$ ,  
2, and 5 (Figure S4). For each  $\tau$ , we computed the WAIC, a criterion for model selection (lower is  
190 better, see Methods), and found WAIC is lowest for  $\tau = 33/32$  and  $\tau = 1$  (Table S3).

Assuming a strong increase of the mutation rate in aneuploid cells, i.e.  $\tau = 100$ , the inferred a  
192 mutation rate was  $\mu = 4.094 \cdot 10^{-7}$  [ $6.252 \cdot 10^{-8} - 6.046 \cdot 10^{-7}$ ]), and the inferred aneuploidy rate  
that was  $\delta = 0.744 \cdot 10^{-3}$  [ $0.506 \cdot 10^{-3} - 1.827 \cdot 10^{-3}$ ]. Compared to inference made assuming  
194 no effect of aneuploidy on the mutation rate, these rates were about 7-8-fold lower about 2-3-fold  
lower. Assuming  $\tau = 10$ , the inferred a mutation rate was only slightly lower compared to  $\tau = 1$   
196 ( $\mu = 1.67 \cdot 10^{-6}$  [ $2.836 \cdot 10^{-8} - 2.245 \cdot 10^{-6}$ ]).

Therefore, we do not find any evidence of an increase in mutation rate in aneuploid cells. This may  
198 be because, unless the increase is strong ( $\tau \geq 10$ ), it does not seem to affect our inference; or because  
chromosome III is one of the smallest chromosomes<sup>16</sup>. We also checked the differences in genotype  
200 frequency dynamics for different  $\tau$  values. We observe  $\tau = 100$  could be distinguished if accurate

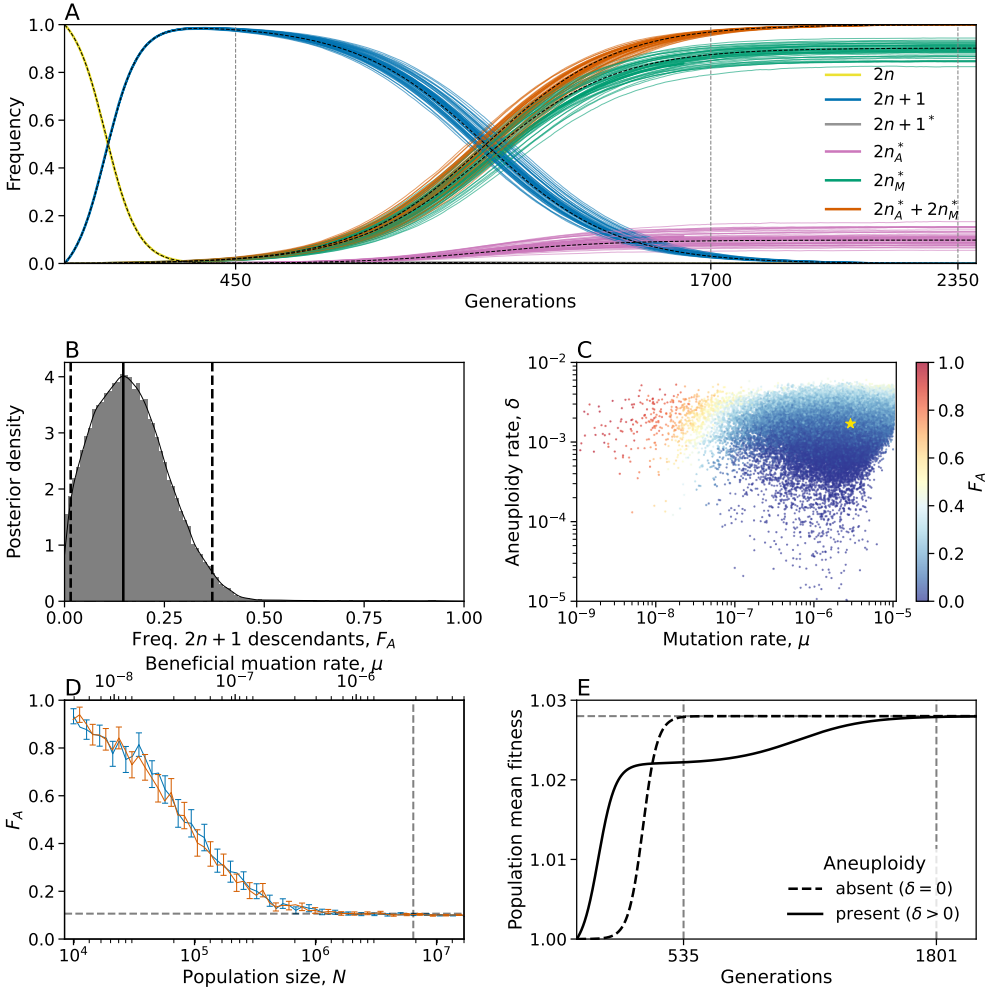


**Figure 5: Predicted frequency of aneuploid-descended cells.** (A) Posterior predicted genotype frequencies over time, including the source of  $2n^*$ :  $2n_A^*$  arose from  $2n+1$ , whereas  $2n_M^*$  arose directly from  $2n$ . Colored curves are 50 simulations using the MAP estimate parameters. Black dashed curves are the expected genotype frequencies without genetic drift (from a deterministic model). See Figure S9 for log-log scale, in which the sequence of events is easier to observe. (B) Posterior distribution of  $F_A$ , the expected frequency of  $2n^*$  cells descended from  $2n+1$  cells, computed as the average frequency at the end of 100 simulations for 100,000 samples from the parameter posterior distribution. Solid and dashed lines show the mode and 95% CI. (C)  $F_A$  values (color coded) from panel B, with their corresponding mutation rate  $\mu$  on x-axis and aneuploidy rate  $\delta$  on the y-axis. Yellow star shows the MAP estimate. See also Figure S10. (D)  $F_A$  as a function of the population size ( $N$ , bottom x-axis) and the beneficial mutation rate ( $\mu$ , top x-axis) in posterior predictions with MAP parameters. Markers show  $F_A$  in 250 simulations per population size or mutation rate value. Error bars show mean  $F_A$  with 95% CI (bootstrap,  $n = 10,000$ ). Blue and red bars for varying population size and mutation rate, respectively. Vertical dashed line for population size in the experiment,  $6.425 \cdot 10^6$ , and the MAP mutation rate,  $2.965 \cdot 10^{-6}$ . Horizontal line for  $F_A^{MAP} = 0.106$ . (E) Population mean fitness in a model without drift using MAP estimate parameters. Solid lines for mean fitness with aneuploidy ( $\delta > 0$ ), where the population reaches adaptation (mean fitness at 99.99% of maximum value) at generation 1,802. Dashed lines for mean fitness without aneuploidy ( $\delta = 0$ ), where the population adapts much earlier, at generation 535.

data was available for the waiting time until the frequency of  $2n$  to decrease below 95% (Figure S5A) 202 or for waiting time for the frequency of  $2n+1$  to either reach or go below 95% (Figure S5B). We also did not find evidence for an increase in the aneuploidy rate in aneuploid cells (data not shown).

## 204 Discussion

In a study on the role of chromosome duplication in adaptive evolution, Yona et al.<sup>62</sup> found that a 206 chromosome III trisomy was acquired by *S. cerevisiae* populations evolving under heat stress, only to be later replaced by euploid mutant cells that carry "refined" solutions to the stress. Additionally, 208 such a replacement also occurred when they initiated evolutionary experiments with a population in which all cells carry a chromosome III trisomy. They hypothesized that aneuploidy is a "useful yet 210 short-lived intermediate that facilitates further adaptation", suggesting that the euploid mutant cells evolved by heat-resistance mutations in aneuploid cells followed by reversion of trisomy due to a 212 chromosome loss event.

If indeed the evolved euploid population is descended from the aneuploid population, then mutant 214 alleles that were common in the aneuploid populations should also be common in the evolved euploid population. However, we found that this is not the case (Figure 1): mutant allele frequencies in the 216 aneuploid and euploid populations are negatively correlated, such that common alleles in the former are rare in the latter. Furthermore, we developed an evolutionary genetic model of adaptive evolution 218 by aneuploidy and mutation (Figure 2), fitted it to the experimental results of Yona et al.<sup>62</sup>, and used it to predict the genotype frequency dynamics. The model predicted that only about 10-15% of 220 the evolved euploid population descended from aneuploid cells—that is, the majority of the euploid population are not descended from aneuploid cells, but rather are direct descendants of the ancestral 222 wild-type population (Figure 5).

This happens despite aneuploidy reaching a high frequency in the population (>95%). Conventional 224 wisdom might suggest that once the aneuploid genotype  $2n+1$  reaches high frequency, it will have a better chance at producing "refined" solutions via mutations, and its descendants will come to dominate 226 the population: the frequency of  $2n_A^*$  (which arises from  $2n+1^*$ ) will be higher than the frequency of  $2n_M^*$  (which arises directly from  $2n$ ).

228 So how does  $2n_M^*$  prevail? Initially, the supply rates of  $2n+1$  and  $2n_M^*$  are  $N\delta \approx 11,000$  and  $N\mu \approx 19$ , respectively (assuming MAP parameter estimates). Therefore, both genotypes are expected to appear 230 immediately at the beginning of the experiment (Figure S9). However,  $2n+1$  appears at a much higher

frequency as  $\delta \gg \mu$  by 2-3 orders of magnitude. After they first appear,  $2n_M^*$  has higher fitness. But  
232 as long as the frequency of  $2n$  is high, the supply rate of  $2n+1$  is higher than that of  $2n_M^*$ , again due to  
 $\delta \gg \mu$ . However, supply rates of both genotypes decreases with the frequency of  $2n$ . Therefore, when  
234 the latter decreases, mainly due to the increase in the frequency of  $2n+1$ , both supply rates diminish.  
At this stage, the higher fitness of  $2n_M^*$  comes into play and it starts to take over the population,  
236 which is mainly composed of  $2n+1$ . For the aneuploid lineage to compete with the mutant lineage, it  
must produce  $2n_A^*$  via a mutation followed by chromosome loss. Although this is a stochastic process  
238 (due to drift), our results show that the time until  $2n_A^*$  reaches a frequency of 0.1% is roughly 450  
generations, without much variation (intersection of purple lines and vertical dashed line in Figure S9).  
240 However, by that time  $2n_M^*$  is already at a roughly 10-fold higher frequency (1.86%), and since both  
mutants have the same fitness, their relative frequency remains roughly the same until the end of the  
242 experiment.

**Predictions for small populations and low mutation rates.** We examined the effect of the popula-  
244 tion size,  $N$ , and the beneficial mutation rate,  $\mu$ , on the frequency of  $2n+1$  descendants in the evolved  
population,  $F_A$ . We found that  $F_A$  is expected to decrease as the population size or mutation rate  
246 increase (Figure 5D), ranging from >90% when the population size is 10,000 or the mutation rate is  
 $6 \cdot 10^{-9}$ , to about 10% when the population size is above 1,000,000 (less than the experimental popu-  
248 lation size, which was 6,425,000) or the mutation rate is above  $2 \cdot 10^{-6}$  (less than the inferred mutation  
rate, which is  $2.965 \cdot 10^{-6}$ ). Thus, our model provides a testable prediction: if the experiment was  
250 repeated under a lower population size (via stronger daily dilutions or in a smaller volume) or a lower  
mutation rate (via a non-mutagenic stress or stress with a smaller target size such as drug resistance),  
252 then the fraction of the population descending from aneuploid cells would be much higher.

**Aneuploidy delays rather than facilitates adaptation.** An additional interesting result of our  
254 study is that aneuploidy increases, rather than decreases, the adaptation time (Figure 5E). This  
happens despite the fact that the mean fitness initially increases faster in the presence of aneuploidy  
256 (Figure 5E). This is because once  $2n+1$  is common, selection for the mutant strain ( $2n+1^*$  or  $2n^*$ ) is  
weaker compared to when  $2n^*$  competes directly with  $2n$ .

258 **Rate and fitness effect of aneuploidy and mutation.** We inferred the rates of aneuploidy and  
mutation and their effects on fitness. We estimate that the aneuploidy rate (i.e., number of chromosome  
260 gains per generation) is  $1.7 \cdot 10^{-3}$ , higher than a previous estimate of  $6.7 \cdot 10^{-6}$  (ref 65). This may be due

to genetic instability caused by heat stress<sup>5</sup>. In addition, we find no evidence for increased mutation  
262 rates in aneuploid cells. Previous empirical studies have suggested that genetic instability (e.g.,  
elevated mutation rates) in aneuploid cells is due to stress associated with the aneuploid state<sup>3,6,63,21</sup>.  
264 However, in the experiment of Yona et al.<sup>62</sup>, both the wild-type and the aneuploid were under heat  
stress, which may explain why we did not find evidence for an increased mutation rate specifically in  
266 aneuploid cells.

**Conclusions.** Here, we tested the hypothesis that aneuploidy cells are an evolutionary "stepping  
268 stone", or adaptive intermediate, between wild-type euploid cells and mutant euploid cells<sup>61</sup>. Our  
results suggest that, although it seems the population goes from euploid to aneuploid and back, this is  
270 not the case at the individual level. We estimate that only about 10-15% of the euploid cells descended  
from aneuploid cells, whereas the rest are direct descendants of the wild-type euploid cells. Thus,  
272 aneuploidy can delay, rather than accelerate, adaptation, and cells that become aneuploid may leave  
less descendants than cells that remain euploid. This surprising result reinforces the importance of  
274 mathematical models when interpreting evolutionary dynamics. Moreover, our study emphasizes the  
unintuitive outcomes of clonal interference between mechanisms for generation of variation that differ  
276 in their rate of formation and distribution of fitness effects, including mutation, copy number variation,  
horizontal gene transfer, and epigenetic modifications.

## 278 Models and Methods

**DNA sequencing.** Whole-genome sequencing of the ancestral diploid strain ( $2n$ ) was performed  
280 on a single colony of the ancestor. Whole-genome sequencing of the four evolving populations ( $H2$   
after 450 and 2,350 generations, and  $H4$  after 450 and 1,700 generations) was performed on a sample  
282 from these populations (rather than from single colonies) in order to maintain the population diversity.  
Cells were grown in 5ml of YPD medium, either at 30 °C (ancestral diploid) or 39 °C (evolved  
284 populations) in shaking conditions (200rpm) until reaching stationary phase. Following growth,  
3ml of each culture were centrifuge (14,000rpm) and cell pellets were used for DNA extraction.  
286 Genomic DNA was extracted using "MasterPure Yeast DNA Purification Kit" (Lucigen) according to  
the manufacture instructions. Following extraction, DNA concentrations were determined by Qubit  
288 assay (Thermo Fisher) and ~ 1 $\mu$ g DNA was used for library preparation using Illumina sample  
preparation kit (Illumina). Samples were sequenced using a 100 bp pair end read output run using  
290 Illumina HiSeq2500.

**Evolutionary genetic model.** We model the evolution of a population of cells using a Wright-Fisher

292 model<sup>35</sup>, assuming a constant effective population size  $N$ , non-overlapping generations, and including  
 the effects of natural selection, genetic drift, aneuploidy, and mutation. We focus on beneficial genetic  
 294 modifications, neglecting the effects of deleterious and neutral mutations or karyotypic changes. The  
 model allows for a single aneuploid karyotype (e.g., chromosome III duplication) and a single mutation  
 296 to accumulate in the genotype. Thus, the model follows four genotypes (Figure 2): euploid wild-type,  
 298  $2n$ , the initial genotype; euploid mutant,  $2n^*$ , with the standard karyotype and a single beneficial muta-  
 tion; aneuploid wild-type,  $2n+1$ , with an extra chromosome, i.e., following chromosome duplication;  
 and aneuploid mutant,  $2n+1^*$ , with an extra chromosome and a beneficial mutation.

300 Transitions between the genotypes occur as follows (Figure 2): Beneficial mutations from  $2n$  to  $2n^*$   
 and from  $2n+1$  to  $2n+1^*$  occur with probability  $\mu$ , the mutation rate. We neglect back-mutations (i.e.,  
 302 from  $2n^*$  to  $2n$  and from  $2n+1^*$  to  $2n+1$ ). Aneuploidy is formed by chromosome mis-segregation,  
 so that cells transition from  $2n$  to  $2n+1$  and from  $2n+1^*$  to  $2n^*$  with probability  $\delta$ , the aneuploidy  
 304 rate. That is, we assume chromosomes are gained and lost at the same rate, and we neglect events  
 that form a less-fit genotype (i.e.,  $2n+1$  to  $2n$  and  $2n^*$  to  $2n+1^*$ ). A model that assumed increased  
 306 aneuploidy rates in aneuploid cells did not perform well and was abandoned.

In the experiment by Yona et al.<sup>62</sup>, the population was grown every day from  $1.6 \cdot 10^6$  cells until  
 308 reaching stationary phase and then diluted 1:120. Thus, we set the population size to  $N = 6.425 \cdot 10^6$ ,  
 the harmonic mean of  $\{2^k \cdot 1.6 \cdot 10^6\}_{k=0}^7$ <sup>9</sup>. The initial population has  $N$  cells with genotype  $2n$ . The  
 310 effect of natural selection on the frequency  $f_i$  of genotype  $i = 2n, 2n + 1, 2n + 1^*$ , or  $2n^*$  is given  
 by

$$312 \quad f_i^s = \frac{f_i w_i}{\bar{w}}, \quad (1)$$

where  $w_i$  is the fitness of genotype  $i$  and  $\bar{w} = \sum_j f_j w_j$  is the population mean fitness. The effect of  
 314 mutation and aneuploidy on genotype frequencies is given by

$$\begin{aligned} f_{2n}^m &= (1 - \delta - \mu)f_{2n}^s, \\ f_{2n+1}^m &= \delta f_{2n}^s + (1 - \mu)f_{2n+1}^s, \\ f_{2n+1^*}^m &= \mu f_{2n+1}^s + (1 - \delta)f_{2n+1^*}^s, \\ f_{2n^*}^m &= \mu f_{2n}^s + \delta f_{2n+1}^s + f_{2n^*}^s. \end{aligned} \quad (2)$$

316 Finally, random genetic drift is modeled using a multinomial distribution<sup>35</sup>,

$$\mathbf{f}' \sim \frac{1}{N} \cdot \text{Mult}(N, \mathbf{f}^m), \quad (3)$$

318 where  $\mathbf{f}^m = (f_{2n}^m, f_{2n+1}^m, f_{2n+1^*}^m, f_{2n^*}^m)$  are the frequencies of the genotypes after mutation and  
 aneuploidy,  $\mathbf{f}'$  are the genotype frequencies in the next generation, and  $\text{Mult}(N, \mathbf{f})$  is a multinomial

320 distribution parameterized by the population size  $N$  and the genotype frequencies  $\mathbf{f}$ . Overall, the change  
in genotype frequencies from one generation to the next is given by the transformation  $f_i \rightarrow f'_i$ .

322 **Empirical data for model inference.** We use the results of evolutionary experiments reported by  
Yona et al.<sup>62</sup>. In their heat-stress experiment, four populations of *S. cerevisiae* evolved under 39 °C.  
324 Aneuploidy fixed in all four population in the first 450 generations. Hereafter, fixation or elimination  
of a genotype by *generation t* means that more than 95% or less than 5% of the population carry the  
326 genotype at generation  $t$ , and possibly earlier. From re-analysis of data not published in the original  
paper, aneuploidy did not fix before at least 200 generations elapsed. The experiment continued with  
328 two populations, in which aneuploidy was eliminated by generation 1,700 and 2,350 while still under  
the same conditions of elevated heat (39 °C).

330 **Likelihood function.** Because our model, just like the Wright-Fisher model, is non-linear and  
stochastic, computing the distribution of fixation time  $T(g)$  of genotype  $g$  for use in the likelihood  
332 function is intractable (it is even hard to use a diffusion-equation approximation due to the model having  
multiple genotypes, rather than just two). We overcome this problem by approximating the likelihood  
334 using simulations. We simulate 1,000 experiments per parameter vector  $\theta = (\mu, \delta, s, b, c)$ , resulting in  
a set of simulated observations  $\tilde{\mathbf{X}} = \{\tilde{X}_i\}_{i=1}^{1000}$ . We then compute the approximate likelihood,

$$\begin{aligned} \mathcal{L}(\theta) = P^4(200 \leq T(2n+1) \leq 450) \cdot & \left[ 1 - \right. \\ & P_{\tilde{\mathbf{X}}}^4(\{T(2n^*) < 1700\} \mid 200 \leq T(2n+1) \leq 450) - \\ & P_{\tilde{\mathbf{X}}}^4(\{1700 < T(2n^*) < 2350\} \mid 200 \leq T(2n+1) \leq 450) + \\ & \left. P_{\tilde{\mathbf{X}}}^4(\{T(2n^*) < 1700\} \wedge \{1700 < T(2n^*) < 2350\} \mid 200 \leq T(2n+1) \leq 450) \right], \end{aligned} \quad (4)$$

where  $\{ \dots \}$  is the "logical not" operator,  $P^4(\dots)$  is the 4th power of  $P(\dots)$ , and all probabilities  
338  $P_{\tilde{\mathbf{X}}}(\dots)$  are approximated from the results of the simulations  $\tilde{\mathbf{X}}$ . For example,  $P_{\tilde{\mathbf{X}}}(\{T(2n^*) < 1700\} \mid$   
 $200 \leq T(2n+1) \leq 450)$  is approximated by taking simulations in which  $2n+1$  fixed before generation  
340 450 but not before generation 200, and computing the fraction of such simulations in which  $2n^*$  did  
not fix by generation 1,700, and hence aneuploidy did not extinct before generation 1,700. Figure S1  
342 compares results with less and more simulated experiments, demonstrating that 1,000 simulations are  
likely sufficient.

344 For a model without aneuploidy (that is, when the aneuploidy rate is fixed at zero,  $\delta = 0$ ), we disregard  
the increased expression in chromosome III and the growth advantage measured in generation 450, and  
346 focus on the growth advantage measured in later generations, presumably due to a beneficial mutation.

Therefore, the likelihood is approximated by

$$\begin{aligned} \mathcal{L}_!(\theta) = 1 - P_{\tilde{\mathbf{X}}}^4(\{T(2n^*) < 1700\}) - \\ 348 \quad P_{\tilde{\mathbf{X}}}^4(\{1700 < T(2n^*) < 2350\}) + \\ P_{\tilde{\mathbf{X}}}^4(\{T(2n^*) < 1700\} \wedge \{1700 < T(2n^*) < 2350\}). \end{aligned} \quad (5)$$

**Parameter inference.** To infer model parameters, we use approximate Bayesian computation with

350 a sequential Monte-Carlo scheme, or ABC-SMC<sup>52</sup>, implemented in the pyABC Python package<sup>26</sup> [pyabc.readthedocs.io](#). This approach uses numerical stochastic simulations of the model to infer  
352 a posterior distribution over the model parameters. It is a method of likelihood-free, simulation-based inference<sup>8</sup>, that is, for estimating a posterior distribution when a likelihood function cannot be  
354 directly computed. It is therefore suitable in our case, in which the likelihood function can only be approximated from simulations, and cannot be directly computed.

356 The ABC-SMC algorithm employs sequential importance sampling over multiple iterations<sup>55,25,53</sup>. In iteration  $t$  of the algorithm, a set of parameter vectors,  $\{\theta_{i,t}\}_{i=1}^{n_t}$ , also called *particles*, are constructed  
358 in the following way. A proposal particle,  $\theta^*$ , is sampled from a proposal distribution, and is either accepted or rejected, until  $n_t$  particles are accepted. The number of particles,  $n_t$ , is adapted at every  
360 iteration  $t$  using the adaptive population strategy<sup>26</sup> [pyabc.readthedocs.io](#). For  $t = 0$ , the proposal particle is sampled from the prior distribution,  $p(\theta)$ . For  $t > 0$ , the proposal particle is sampled from  
362 the particles accepted in the previous iteration,  $\{\theta_{i,t-1}\}_{i=1}^{n_{t-1}}$ , each with a probability relative to its weight  
364  $W_{t-1}(\theta_{i,t-1})$  (see below). The proposal particle is then perturbed using a kernel perturbation kernel,  
366  $K_t(\theta^* | \theta)$  where  $\theta$  is the sample from the previous iteration. Then, a set of synthetic observations  
368  $\tilde{\mathbf{X}}^*$  is simulated, and the proposal particle  $\theta^*$  is accepted if its approximate likelihood (eq. (4)) is high  
370 enough,  $\mathcal{L}(\theta^*) > 1 - \epsilon_t$  (or more commonly, if  $1 - \mathcal{L}(\theta^*) < \epsilon_t$ ), where  $\epsilon_t > 0$  is the *acceptance threshold*, as higher values of  $\epsilon_t$  allow more particles to be accepted. The acceptance threshold  $\epsilon_t$   
372 is chosen as the median of the  $1 - \mathcal{L}(\theta)$  of the particles accepted in the previous iteration,  $t - 1$ , and  $\epsilon_0 = 0.01$ . For each accepted particle  $\theta_{i,t}$  a weight  $W_t(\theta_{i,t})$  is assigned: for  $t = 0$ ,  $W_0(\theta_{i,0}) = 1$ ,  
374 and for  $t > 0$ ,  $W_t(\theta_{i,t}) = p(\theta_{i,t}) / \sum_{i=1}^{n_{t-1}} W_{t-1}(\theta_{i,t-1}) K_t(\theta_{i,t}, \theta_{i,t-1})$ , where  $p(\theta)$  is the prior density of  $\theta$  and  $K_t(\theta', \theta)$  is the probability of a perturbation from  $\theta$  to  $\theta'$ .  $K_t(\theta' | \theta)$  is a multivariate normal  
376 distribution, fitted at iteration  $t$  to the particles from the previous iteration,  $\{\theta_{i,t-1}\}_{i=1}^{n_{t-1}}$ , and their weights,  $\{W(\theta_{i,t-1})\}_{i=1}^{n_{t-1}}$ .

374 Acceptance is determined according to the approximate likelihood (eq. (4)), which has a maximum value of  $\mathcal{L}_{max} = 0.875$  (giving a minimal value of  $\epsilon_{min} = 0.125$ ). We terminated the inference  
376 iterations when the change in  $\epsilon$  value from one iteration to the next was small. With our standard prior

and model, we reached  $\epsilon = 0.13$  (or  $\mathcal{L} = 0.87$ ) after six iterations, with  $n_6 = 982$  accepted parameter  
378 vectors and effective sample size ESS=651 (Figure S2). Running the inference algorithm with different  
initialization seeds and less or more simulations for approximating the likelihood produced similar  
380 posterior distributions (Figure S1).

After producing a set of weighted particles from the the posterior distribution using the above ABC-SMC  
382 algorithm, we approximate the posterior using kernel density estimation (KDE) with Gaussian  
kernels. We truncate the estimated posterior to avoid positive posterior density for values with zero  
384 prior density. The MAP (maximum a posteriori) estimate is computed as the the maximum of the  
estimated joint posterior density. We then draw 5,000,000 samples from the posterior distribution  
386 to compute the HDI (highest density interval) and draw 50,000 samples to visualize the posterior  
distribution with histograms.

388 **Model comparison.** We examine several versions of our evolutionary models, e.g. without aneuploidy or with increased mutation rate in aneuploid cells, as well as several different prior distributions  
390 (see below). To compare these, we plot posterior predictions: for each model we execute 10,000  
simulations using the MAP parameter estimates and plot the distributions of time to fixation of  $2n^*$ ,  
392 one of key properties of the model likelihood. These plots visualize the fit of each model to the  
data. Also, for similar models we plot the marginal and joint posterior distributions of the parameters;  
394 if these are similar, we consider the models interchangeable. We validate this by comparing HDI  
(highest density interval) of posterior distributions.

396 Where posterior plots are very similar and the number of parameters is the same, we use WAIC, or  
the widely applicable information criterion <sup>13</sup>, defined as

$$398 \quad WAIC(\theta) = -2 \log \mathbb{E}[\mathcal{L}(\theta)] + 2\mathbb{V}[\log \mathcal{L}(\theta)] \quad (6)$$

where  $\theta$  is a parameter vector, and  $\mathbb{E}[\cdot]$  and  $\mathbb{V}[\cdot]$  are the expectation and variance taken over the  
400 posterior distribution, which in practice are approximated using 50,000 samples from the posterior  
KDE. We validated that upon resampling WAIC values do not significantly change and that differences  
402 in WAIC between models are preserved. WAIC values are scaled as a deviance measure: lower values  
imply higher predictive accuracy<sup>23</sup>.

404 **Prior distributions.** We used informative prior distributions for  $w_{2n+1} = 1 - c + b$ ,  $w_{2n+1^*} =$   
 $(1+s)(1-c)+b$  and  $w_{2n^*} = 1+s$ , which we estimated from growth curves data from mono-culture growth  
406 experiments previously reported by Yona et al.<sup>62</sup>, Figs. 3C, 4A, and S2. We used Curveball, a method

for predicting results of competition experiments from growth curve data<sup>38</sup> [curveball.yoavram.com](http://curveball.yoavram.com).  
408 Briefly, Curveball takes growth curves of two strains growing separately in mono-culture and predicts  
how they would grow in a mixed culture, that is, it predicts the results of a competition assay. From these  
410 predictions, relative fitness values can be computed. Because Curveball uses a maximum-likelihood  
approach to estimate model parameters, we were able to estimate a distribution of relative fitness  
412 values to be used as a prior distribution by sampling 10,000 samples from a truncated multivariate  
normal distribution defined by the maximum-likelihood covariance matrix (Figure S3).  
  
414 We used growth curves of  $2n$  and  $2n+1$  in 39 °C to estimate an informative prior distribution for  
 $w_{2n+1}$  (Figure S3-D, assuming  $w_{2n} = 1$ ). In this prior distribution, we used the same prior for  $w_{2n+1*}$   
416 and  $w_{2n*}$ . To increase computational efficiency, we also assumed  $w_{2n*} > w_{2n+1*} > w_{2n+1} > w_{2n}$ ;  
running the inference without this assumption produced similar results. See *supporting material* for  
418 an extended informative prior distribution that uses growth curves of  $2n^*$  and  $2n+1$  growing in 39 °C;  
this prior distribution proved to be less useful.  
  
420 As a control, we tested an uninformative uniform prior with  $U(1, 6)$ , for (i) all  $w_{2n+1}$ ,  $w_{2n+1*}$ ,  $w_{2n*}$ , or  
(ii) only for  $w_{2n+1*}$ ,  $w_{2n*}$ , using the above informative prior for  $w_{2n+1}$ . In these cases the inference  
422 algorithm failed to converge.

For the mutation rate,  $\mu$ , and aneuploidy rate,  $\delta$ , we used uninformative uniform priors,  $\mu \sim$   
424  $U(10^{-9}, 10^{-5})$  and  $\delta \sim U(10^{-6}, 10^{-2})$ . A wider mutation rate prior,  $\mu \sim U(10^{-9}, 10^{-3})$ , produced  
similar results.

## 426 Acknowledgements

We thank Lilach Hadany, Judith Berman, David Gresham, Shay Covo, Martin Kupiec, Uri Obolski, Daniel  
428 Weissman, and Tal Simon for discussions and comments. This work was supported in part by the Israel  
Science Foundation (ISF, YR 552/19), the US–Israel Binational Science Foundation (BSF, YR 2021276),  
430 Minerva Center for Live Emulation of Evolution in the Lab (YP, YR), Minerva Stiftung short-term research  
grant (MP).

## 432 References

- [1] Avecilla, G., Chuong, J. N., Li, F., Sherlock, G., Gresham, D. and Ram, Y. 2022, ‘Neural  
434 networks enable efficient and accurate simulation-based inference of evolutionary parameters  
from adaptation dynamics’, *PLOS Biology* **20**(5), e3001633.

- 436 [2] Bakhoum, S. F. and Landau, D. A. 2017, ‘Chromosomal instability as a driver of tumor heterogeneity and evolution’, *Cold Spring Harb. Perspect. Med.* **7**(6), 1–14.
- 438 [3] Bouchonville, K., Forche, A., Tang, K. E. S., Semple, C. a. M. and Berman, J. 2009, ‘Aneuploid chromosomes are highly unstable during dna transformation of *Candida albicans*.’, *Eukaryot. Cell* **8**(10), 1554–66.
- 440 [4] Boveri, T. 2008, ‘Concerning the origin of malignant tumours’, *J. Cell Sci.* **121**(Supplement 1), 1–84.
- 442 [5] Chen, G., Bradford, W. D., Seidel, C. W. and Li, R. 2012, ‘Hsp90 stress potentiates rapid cellular adaptation through induction of aneuploidy.’, *Nature* **482**(7384), 246–50.
- 444 [6] Chen, G., Rubinstein, B. and Li, R. 2012, ‘Whole chromosome aneuploidy: Big mutations drive adaptation by phenotypic leap’, *BioEssays* **34**(10), 893–900.
- 446 [7] Covo, S., Puccia, C. M., Argueso, J. L., Gordenin, D. A. and Resnick, M. A. 2014, ‘The sister chromatid cohesion pathway suppresses multiple chromosome gain and chromosome amplification.’, *Genetics* **196**(2), 373–384.
- 450 [8] Cranmer, K., Brehmer, J. and Louppe, G. 2020, ‘The frontier of simulation-based inference’, *Proceedings of the National Academy of Sciences* p. 201912789.
- 452 [9] Crow, J. F. and Kimura, M. 1970, *An introduction to population genetics theory*, Burgess Pub. Co., Minneapolis.
- 454 [10] Dhar, R. and Sägesser, R and Weikert, C and Yuan, J and Wagner, Andreas, doi = 10.1111/j.1420-9101.2011.02249.x, i . . j. . J. m. . m. n. . p. . p. . t. . A. v. . y. . n.d..
- 456 [11] Dunham, M. J., Badrane, H., Ferea, T., Adams, J., Brown, P. O., Rosenzweig, F. and Botstein, D. 2002, ‘Characteristic genome rearrangements in experimental evolution of *Saccharomyces cerevisiae*’, *Proc. Natl. Acad. Sci.* **99**(25), 16144–16149.
- 460 [12] Flynn, J. M., Rossouw, A., Cote-Hammarlof, P., Fragata, I., Mavor, D., Hollins, C., Bank, C. and Bolon, D. N. 2020, ‘Comprehensive fitness maps of hsp90 show widespread environmental dependence’, *Elife* **9**, 1–25.
- 462 [13] Gelman, A., Carlin, J. B., Stern, H. S., Dunson, D. B., Vehtari, A. and Rubin, D. B. 2013, *Bayesian Data Analysis, Third Edition*, Chapman & Hall/CRC Texts in Statistical Science, Taylor & Francis.

- 466 [14] Gerstein, A. C. and Berman, J. 2018, ‘Diversity of acquired adaptation to fluconazole is influenced  
by genetic background and ancestral fitness in *Candida albicans*’, *bioRxiv* p. 360347.
- 468 [15] Gerstein, A. C., Ono, J., Lo, D. S., Campbell, M. L., Kuzmin, A. and Otto, S. P. 2015, ‘Too  
much of a good thing: the unique and repeated paths toward copper adaptation.’, *Genetics*  
**199**(2), 555–71.
- 470 [16] Gilchrist, C. and Stelkens, R. 2019, ‘Aneuploidy in yeast: Segregation error or adaptation  
mechanism?’, *Yeast* **36**(9), 525–539.
- 472 [17] Gresham, D., Desai, M. M., Tucker, C. M., Jenq, H. T., Pai, D. A., Ward, A., DeSevo, C. G.,  
Botstein, D. and Dunham, M. J. 2008, ‘The repertoire and dynamics of evolutionary adaptations  
474 to controlled nutrient-limited environments in yeast’, *PLoS Genet.* **4**(12).
- 476 [18] Heidenreich, E. 2007, ‘Adaptive Mutation in *< i>Saccharomyces cerevisiae</i>*’, *Crit. Rev.  
Biochem. Mol. Biol.* **42**(4), 285–311.
- 478 [19] Hong, J. and Gresham, D. 2014, ‘Molecular specificity, convergence and constraint shape adap-  
tive evolution in nutrient-poor environments’, *PLoS Genet.* **10**(1).
- 480 [20] Huang, C. J., Lu, M. Y., Chang, Y. W. and Li, W. H. 2018, ‘Experimental Evolution of Yeast for  
High-Temperature Tolerance’, *Mol. Biol. Evol.* **35**(8), 1823–1839.
- 482 [21] Ippolito, M. R., Martis, V., Martin, S., Tijhuis, A. E., Hong, C., Wardenaar, R., Dumont,  
M., Zerbib, J., Spierings, D. C., Fachinetti, D., Ben-David, U., Fojer, F. and Santaguida, S.  
2021, ‘Gene copy-number changes and chromosomal instability induced by aneuploidy confer  
484 resistance to chemotherapy’, *Dev. Cell* **56**(17), 2440–2454.e6.
- 486 [22] Iwasa, Y., Michor, F. and Nowak, M. A. 2004, ‘Stochastic tunnels in evolutionary dynamics’,  
*Genetics* **166**(3), 1571–1579.
- 488 [23] Kass, R. E. and Raftery, A. E. 1995, ‘Bayes factors’, *J. Am. Stat. Assoc.* **90**(430), 773.
- 490 [24] Kasuga, T., Bui, M., Bernhardt, E., Swiecki, T., Aram, K., Cano, L. M., Webber, J., Brasier,  
C., Press, C. and Grünwald, Niklaus J. and Rizzo, David M. and Garbelotto, Matteo, doi  
= 10.1186/s12864-016-2717-z, i . . . i . . . j . . B. n . . . p . . . p . . p . . B. t . . H. v . . . y . . n.d..
- 492 [25] Klinger, E. and Hasenauer, J. 2017, A scheme for adaptive selection of population sizes in  
approximate bayesian computation - sequential monte carlo, *in* J. Feret and H. Koepll, eds,  
‘Computational Methods in Systems Biology’, Vol. 10545, Springer International Publishing,  
494 pp. 128–144. Series Title: Lecture Notes in Computer Science.

- [26] Klinger, E., Rickert, D. and Hasenauer, J. 2018, ‘pyabc: distributed, likelihood-free inference’,  
496        *Bioinformatics* (May), 1–3.
- [27] Kohn, L. M. and Anderson, J. B. 2014, ‘The underlying structure of adaptation under strong  
498        selection in 12 experimental yeast populations’, *Eukaryot. Cell* **13**(9), 1200–1206.
- [28] Komarova, N. L., Sengupta, A. and Nowak, M. A. 2003, ‘Mutation-selection networks of cancer  
500        initiation: Tumor suppressor genes and chromosomal instability’, *J. Theor. Biol.* **223**(4), 433–  
450.
- 502 [29] Kumaran, R., Yang, S.-Y. and Leu, J.-Y. n.d., ‘Characterization of chromosome stability in  
diploid, polyploid and hybrid yeast cells’, **8**(7), e68094.
- 504 [30] Lynch, M., Sung, W., Morris, K., Coffey, N., Landry, C. R., Dopman, E. B., Dickinson, W. J.,  
Okamoto, K., Kulkarni, S., Hartl, D. L. and Thomas, W. K. 2008, ‘A genome-wide view of the  
506        spectrum of spontaneous mutations in yeast’, *Proceedings of the National Academy of Sciences*  
**105**(27), 9272–9277.
- 508 [31] Mannaert, A., Downing, T., Imamura, H. and Dujardin, J. C. 2012, ‘Adaptive mechanisms in  
pathogens: Universal aneuploidy in *Leishmania*’, *Trends Parasitol.* **28**(9), 370–376.
- 510 [32] Möller, M., Habig, M., Freitag, M. and Stukenbrock, E. H. 2018, ‘Extraordinary genome  
instability and widespread chromosome rearrangements during vegetative growth’, *Genetics*  
512        **210**(2), 517–529.
- 514 [33] Naylor, R. M. and van Deursen, J. M. 2016, ‘Aneuploidy in cancer and aging’, *Annu. Rev. Genet.*  
**50**(1), 45–66.
- 516 [34] Niwa, O., Tange, Y. and Kurabayashi, A. 2006, ‘Growth arrest and chromosome instability in  
aneuploid yeast’, *Yeast* **23**(13), 937–950.
- 518 [35] Otto, S. P. and Day, T. 2007, *A biologist’s guide to mathematical modeling in ecology and  
evolution*, Princeton University Press.
- 520 [36] Pavelka, N., Rancati, G., Zhu, J., Bradford, W. D., Saraf, A., Florens, L., Sanderson, B. W., Hat-  
tem, G. L. and Li, R. 2010, ‘Aneuploidy confers quantitative proteome changes and phenotypic  
variation in budding yeast.’, *Nature* **468**(7321), 321–5.
- 522 [37] Peter, J., De Chiara, M., Friedrich, A., Yue, J. X., Pflieger, D., Bergström, A., Sigwalt, A., Barre,  
B., Freel, K., Llored, A., Cruaud, C., Labadie, K., Aury, J. M., Istace, B., Lebrigand, K., Barbry,

- 524 P., Engelen, S., Lemainque, A., Wincker, P., Liti, G. and Schacherer, J. 2018, ‘Genome evolution  
across 1,011 <i>Saccharomyces cerevisiae</i> isolates’, *Nature* **556**(7701), 339–344.
- 526 [38] Ram, Y., Dellus-Gur, E., Bibi, M., Karkare, K., Obolski, U., Feldman, M. W., Cooper, T. F.,  
Berman, J. and Hadany, L. 2019, ‘Predicting microbial growth in a mixed culture from growth  
528 curve data’, *Proceedings of the National Academy of Sciences* **116**(29), 14698–14707.
- 530 [39] Rancati, G., Pavelka, N., Fleharty, B., Noll, A., Trimble, R., Walton, K., Perera, A., Staehling-  
Hampton, K., Seidel, C. W. and Li, R. 2008, ‘Aneuploidy underlies rapid adaptive evolution of  
yeast cells deprived of a conserved cytokinesis motor’, *Cell* **135**(5), 879–893.
- 532 [40] Robbins, N., Caplan, T. and Cowen, L. E. 2017, ‘Molecular evolution of antifungal drug resis-  
tance’, *Annu. Rev. Microbiol.* **71**(1), 753–775.
- 534 [41] Rodrigues, M. L. and Albuquerque, P. C. 2018, ‘Searching for a change: The need for increased  
support for public health and research on fungal diseases’, *PLoS Negl. Trop. Dis.* **12**(6), 1–5.
- 536 [42] Santaguida, S. and Amon, A. 2015, ‘Short- and long-term effects of chromosome mis-segregation  
and aneuploidy’, *Nat. Rev. Mol. Cell Biol.* **16**(8), 473–485.
- 538 [43] Santaguida, S., Vasile, E., White, E. and Amon, A. 2015, ‘Aneuploidy-induced cellular stresses  
limit autophagic degradation’, *Genes Dev.* **29**(19), 2010–2021.
- 540 [44] Schwartzman, J. M., Sotillo, R. and Benezra, R. 2010, ‘Mitotic chromosomal instability and  
cancer: Mouse modelling of the human disease’, *Nat. Rev. Cancer* **10**(2), 102–115.
- 542 [45] Selmecki, A. M., Dulmage, K., Cowen, L. E., Anderson, J. B. and Berman, J. 2009, ‘Acquisition  
of aneuploidy provides increased fitness during the evolution of antifungal drug resistance’, *PLoS  
544 Genet.* **5**(10), e1000705.
- 546 [46] Selmecki, A. M., Forche, A. and Berman, J. 2010, ‘Genomic plasticity of the human fungal  
pathogen *Candida albicans*’, *Eukaryot. Cell* **9**(7), 991–1008.
- 548 [47] Selmecki, A. M., Gerami-Nejad, M., Paulson, C., Forche, A. and Berman, J. 2008, ‘An isocho-  
mosome confers drug resistance in vivo by amplification of two genes, erg11 and tac1’, *Mol.  
Microbiol.* **68**(3), 624–641.
- 550 [48] Sheltzer, J. M. and Amon, A. 2011, ‘The aneuploidy paradox: Costs and benefits of an incorrect  
karyotype’, *Trends Genet.* **27**(11), 446–453.
- 552 [49] Sheltzer, J. M., Blank, H. M., Pfau, S. J., Tange, Y., George, B. M., Humpton, T. J., Brito, I. L.,

- Hiraoka, Y., Niwa, O. and Amon, A. 2011, 'Aneuploidy drives genomic instability in yeast',  
554 *Science* **333**(6045), 1026–1030.
- [50] Sheltzer, J. M., Ko, J. H., Replogle, J. M., Habibe Burgos, N. C., Chung, E. S., Meehl, C. M.,  
556 Sayles, N. M., Passerini, V., Storchova, Z. and Amon, A. 2017, 'Single-chromosome gains  
commonly function as tumor suppressors', *Cancer Cell* **31**(2), 240–255.
- 558 [51] Sionov, E., Lee, H., Chang, Y. C. and Kwon-Chung, K. J. 2010, '*Cryptococcus neoformans*  
overcomes stress of azole drugs by formation of disomy in specific multiple chromosomes',  
560 *PLoS Pathog.* **6**(4), e1000848.
- [52] Sisson, S. A., Fan, Y. and Tanaka, M. M. 2007, 'Sequential monte carlo without likelihoods',  
562 *Proceedings of the National Academy of Sciences* **104**(6), 1760–1765.
- [53] Syga, S., David-Rus, D. and Schälte, Yannik and Hatzikirou, Haralampos and Deutsch, Andreas,  
564 doi = 10.1038/s41598-021-01407-y, j. . S. n. . p. . t. . I. v. . y. . n.d..
- [54] Todd, R. T., Forche, A. and Selmecki, A. M. 2017, 'Ploidy variation in fungi: Polyploidy,  
566 aneuploidy, and genome evolution', *Microbiol. Spectr.* **5**(4), 1–20.
- [55] Toni, T., Welch, D., Strelkowa, N., Ipsen, A. and Stumpf, M. P. 2009, 'Approximate bayesian  
568 computation scheme for parameter inference and model selection in dynamical systems', *J. R.  
Soc. Interface* **6**(31), 187–202.
- 570 [56] Torres, E. M., Dephoure, N., Panneerselvam, A., Tucker, C. M., Whittaker, C. A., Gygi, S. P.,  
Dunham, M. J. and Amon, A. 2010, 'Identification of aneuploidy-tolerating mutations', *Cell*  
572 **143**(1), 71–83.
- [57] Torres, E. M., Sokolsky, T., Tucker, C. M., Chan, L. Y., Boselli, M., Dunham, M. J. and Amon,  
574 A. 2007, 'Effects of aneuploidy on cellular physiology and cell division in haploid yeast', *Science*  
(80-. ). **317**(5840), 916–924.
- 576 [58] Tsai, H. J., Nelliat, A. R., Choudhury, M. I., Kucharavy, A., Bradford, W. D., Cook, M. E., Kim,  
J., Mair, D. B., Sun, S. X., Schatz, M. C. and Li, R. 2019, 'Hypo-osmotic-like stress underlies  
578 general cellular defects of aneuploidy', *Nature* .
- [59] Williams, B. R., Prabhu, V. R., Hunter, K. E., Glazier, C. M., Whittaker, C. a., Housman,  
580 D. E. and Amon, A. 2008, 'Aneuploidy affects proliferation and spontaneous immortalization in  
mammalian cells', *Science* **322**(5902), 703–709.

- 582 [60] Yang, F., Todd, R. T., Selmecki, A., Jiang, Y. Y., Cao, Y. B. and Berman, J. 2021, ‘The fitness  
costs and benefits of trisomy of each *Candida albicans* chromosome’, *Genetics* **218**(2), 1–7.
- 584 [61] Yona, A. H., Frumkin, I. and Pilpel, Y. 2015, ‘A relay race on the evolutionary adaptation  
spectrum’, *Cell* **163**(3), 549–559.
- 586 [62] Yona, A. H., Manor, Y. S., Herbst, R. H., Romano, G. H., Mitchell, A., Kupiec, M., Pilpel, Y.  
and Dahan, O. 2012, ‘Chromosomal duplication is a transient evolutionary solution to stress.’,  
588 *Proceedings of the National Academy of Sciences* **109**(51), 21010–5.
- 590 [63] Zhu, J., Pavelka, N., Bradford, W. D., Rancati, G. and Li, R. 2012, ‘Karyotypic determinants of  
chromosome instability in aneuploid budding yeast’, *PLoS Genetics* **8**(5).
- 592 [64] Zhu, J., Tsai, H.-J., Gordon, M. R. and Li, R. 2018, ‘Cellular stress associated with aneuploidy’,  
*Dev. Cell* **44**(4), 420–431.
- 594 [65] Zhu, Y. O., Sherlock, G. and Petrov, D. A. 2016, ‘Whole genome analysis of 132 clinical *Sac-*  
*charomyces cerevisiae* strains reveals extensive ploidy variation’, *G3 Genes, Genomes, Genetics*  
**6**(8), 2421–2434.
- 596 [66] Zhu, Y. O., Siegal, M. L., Hall, D. W. and Petrov, D. A. 2014, ‘Precise estimates of mutation rate  
and spectrum in yeast’, *Proceedings of the National Academy of Sciences* **111**(22), E2310–E2318.

## 598 Supplementary Material

### Supplementary Analysis

600 **Sensitivity analysis.** Changing a single parameter while keeping the rest fixed at the MAP estimate produces a worse fit to the data (Figure S6). Furthermore, we fitted models with a mutation rate  
602 fixed at  $\mu = 10^{-5}$ ,  $10^{-6}$  and  $10^{-7}$ . We inferred similar parameters estimates for the model with  
604  $\mu = 10^{-6}$  compared to the model with a free  $\mu$  parameter, in which the inferred mutation rate is  
 $\mu \approx 3 \cdot 10^{-6}$ . Inference assuming  $\mu = 10^{-5}$  or  $\mu = 10^{-7}$  produced similar estimates except that the  
estimated aneuploidy rate,  $\delta$ , was higher, and assuming  $\mu = 10^{-7}$ , the estimated fitness of  $2n+1$  was  
606 lower (Figure S7).

**Extended informative prior distribution.** In an extended informative prior distribution, we used  
608 additional growth curves of  $2n^*$  (*refined* strain from Yona et al.<sup>62</sup>) and  $2n+1$  in 39 °C to estimate  
 $w_{2n^*}/w_{2n+1}$  (Figure S3L). The same distribution was used for  $w_{2n^*}/w_{2n+1*}$ . Thus, our main infor-  
610 mative prior uses a single prior distribution for fitness values of  $2n+1$ ,  $2n+1^*$ , and  $2n^*$ , whereas the  
extended informative prior uses one distribution for  $2n+1$ , and another distribution for both  $2n+1^*$   
612 and  $2n^*$ .

We estimated the parameters under this extended informative prior. Inference took much longer  
614 to run but the posterior distribution seemed to converge, as it did not change much in the final  
iterations. The posterior predictive plot shows that inference with this extended prior produces a  
616 posterior distribution that fails to explain the empirical observations (pink in Figure 4). However,  
the inferred posterior distribution is considerably narrower (compare Figures 3 and S8) and therefore  
618 parameter estimates are less variable. The estimated mutation rate was much lower compared to  
the main informative prior, with  $\mu = 2.474 \cdot 10^{-9}$  [ $2.423 \cdot 10^{-9} - 2.612 \cdot 10^{-9}$ ]. Other parameter  
620 estimates are:  $\delta = 2.705 \cdot 10^{-3}$  [ $2.094 \cdot 10^{-3} - 3.094 \cdot 10^{-3}$ ],  $w_{2n+1} = 1.022$  [ $1.021 - 1.024$ ],  
 $w_{2n+1*} = 1.052$  [ $1.05 - 1.054$ ],  $w_{2n^*} = 1.053$  [ $1.051 - 1.055$ ], the latter two being much higher  
622 compare to the main informative prior. Notably, the mode of the posterior ratio  $w_{2n^*}/w_{2n+1} = 1.0009$   
is much lower than the mode of the prior ratio of 1.033 (Figure S3H) and closer to the ratio of 1 that  
624 we assume in the main informative prior. Together with the posterior predictive results, we conclude  
that the main informative prior is preferable over the extended informative prior.

626 **Model with transitions to less-fit genotypes** We also estimated the parameters of a version of the  
 model that includes transitions (mutation, chromosome loss and gain) to less-fit genotypes (e.g.,  $2n^*$   
 628 to  $2n+1^*$ ),

$$\begin{aligned} f_{2n}^m &= (1 - \delta - \mu)f_{2n}^s + \delta f_{2n+1}^s + \mu f_{2n+1}^s, \\ f_{2n+1}^m &= \delta f_{2n}^s + (1 - \delta - \mu)f_{2n+1}^s + \mu f_{2n+1}^s, \\ f_{2n+1}^m &= \mu f_{2n+1}^s + (1 - \delta - \mu)f_{2n+1}^s + \delta f_{2n}^s, \\ f_{2n}^m &= \mu f_{2n}^s + \delta f_{2n+1}^s + (1 - \delta - \mu)f_{2n}^s. \end{aligned} \tag{7}$$

630 The inferred values are slightly different. The estimated mutation rate,  $\mu = 1.036 \cdot 10^{-7}$  [ $8.01 \cdot 10^{-8} - 1.339 \cdot 10^{-7}$ ], corresponds to a mutation target size of  $\sim 300 - 500$ , assuming the mutation  
 632 rate per base pair is roughly  $2 \cdot 10^{-10}$  (ref.<sup>66</sup>) or  $3.3 \cdot 10^{-10}$  (ref.<sup>30</sup>). The estimated aneuploidy  
 634 rate,  $\delta = 2.358 \cdot 10^{-4}$  [ $1.766 \cdot 10^{-4} - 2.837 \cdot 10^{-4}$ ] is 5-35-fold higher than in previous studies:  
 636 for chromosome III in diploid *S. cerevisiae*, Zhu et al.<sup>66</sup> estimated  $6.7 \cdot 10^{-6}$  chromosome gain  
 events per generation, and Kumaran et al.<sup>29</sup> estimate  $3.0 - 4.3 \cdot 10^{-5}$  chromosome loss events per  
 638 generation (95% confidence interval). The estimated fitness values are  $w_{2n+1} = 1.024$  [1.023 – 1.025],  
 $w_{2n+1}^* = 1.025$  [1.024 – 1.026],  $w_{2n}^* = 1.032$  [1.031 – 1.033], all relative to the fitness of  $2n$ , which  
 640 is set to  $w_{2n} = 1$ . Thus, we can infer that the cost of trisomy is  $c = w_{2n}^* - w_{2n+1}^* = 0.007$  (or 0.7%)  
 and the benefit of trisomy is  $w_{2n+1} - 1 - c = 0.017$  (1.7%), whereas the benefit of beneficial mutation  
 is  $w_{2n}^* - 1 = 0.032$  (3.2%).

We simulated genotype frequency dynamics using parameter samples from the posterior distribution,  
 642 and computed the posterior distribution of  $F_A$ . The mean  $F_A$  in this case is just 0.0189 [0.0004 - 0.1214  
 95% CI], lower than without the transitions to less-fit genotypes. Here,  $F_A$  is the sum of frequencies  
 644 of both  $2n_A^*$  and  $2n + 1_A^*$ , which reaches a frequency of 0.0007. Out of 100,000 posterior samples,  
 none had  $F_A$  above 0.05 (i.e., 5% of the population).

646 **Supplementary Figures & Tables**

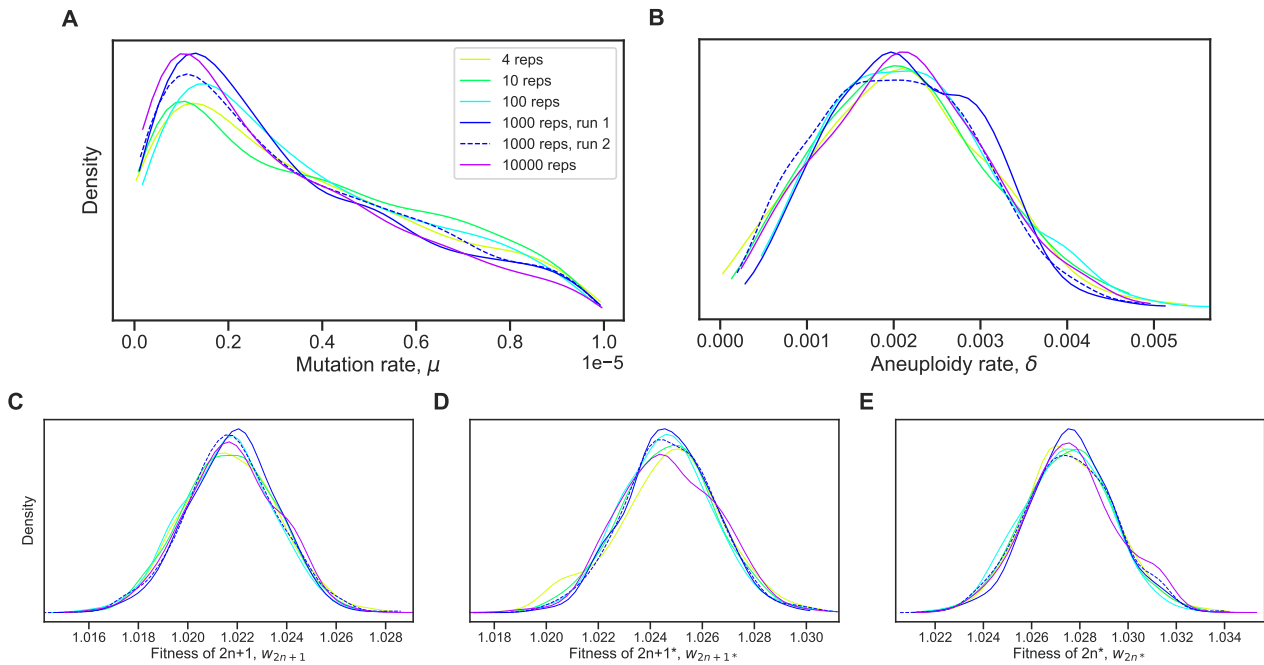


**Figure S1: Posterior distribution validation.** The posterior distribution of model parameters is roughly the same regardless of the number of simulations (4-10,000 replicates) used to approximate the likelihood (eq. (4)).

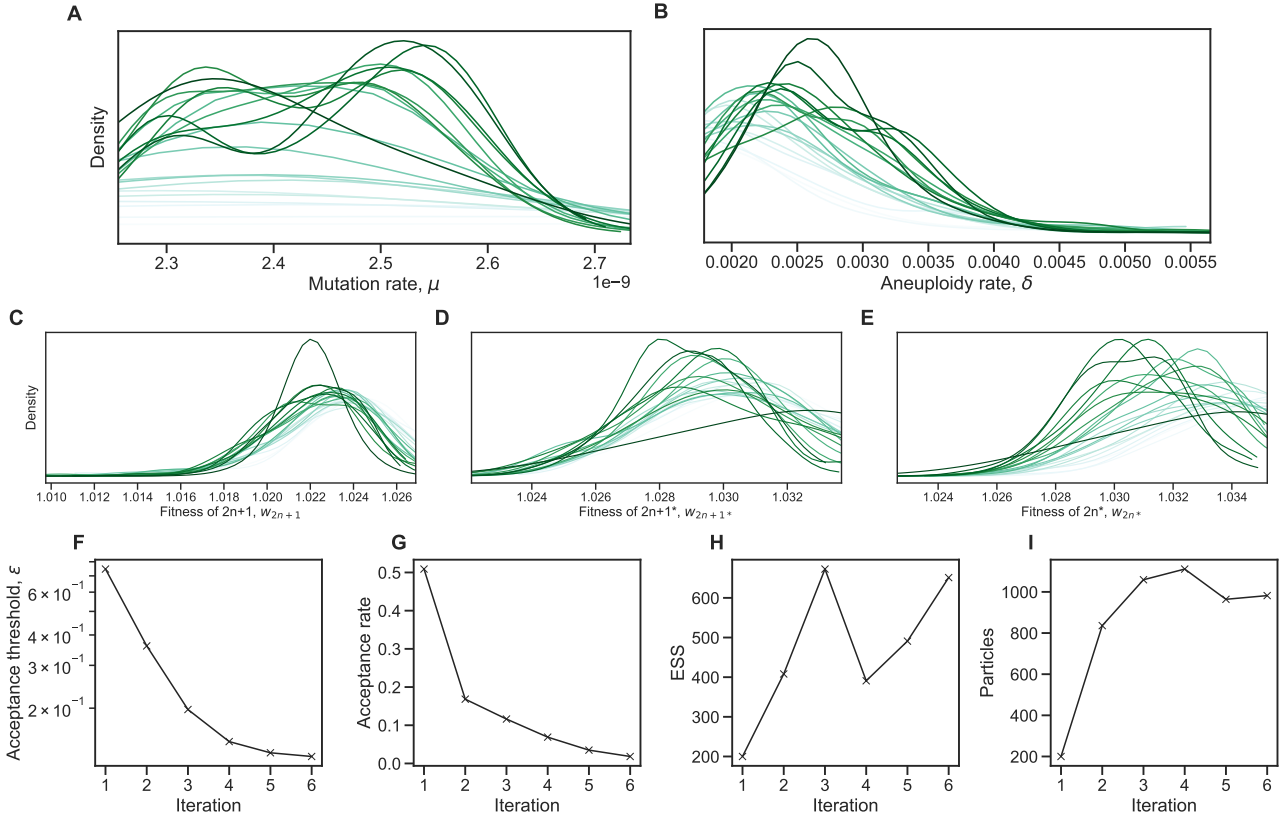


**Figure S2: Inference convergence.** The ABC-SMC algorithm was used to infer the model parameters. **(A-E)** The approximate posterior distributions of model parameters at each iteration of the ABC-SMC algorithm demonstrates convergence, as the posterior did not significantly change after the first iteration,  $t = 1$ . **(F-I)** ABC-SMC measures of convergence. After iteration number 6, the acceptance threshold was  $\epsilon = 0.13$  (i.e.,  $\mathcal{L} = 0.87$ , eq. (4)), the acceptance rate was 0.018, the number of particles was 982, and the effective sample size ESS=651.

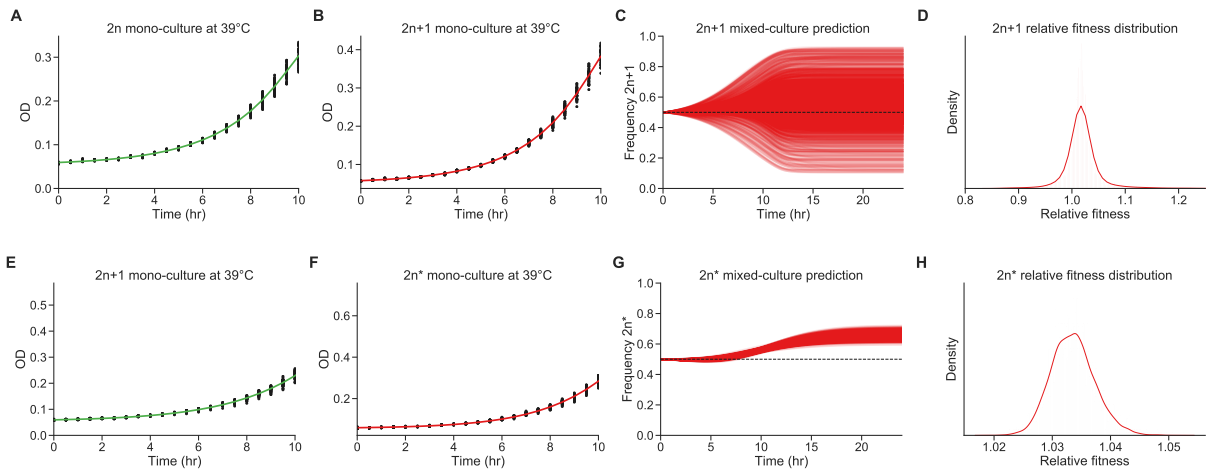


**Figure S3: Fitness estimation from growth curves.** **(A-D)** Fitness estimation from growth curves of  $2n$  and  $2n+1$  at  $39^{\circ}\text{C}$ .  $w_{2n+1}/w_{2n}=1.024$  (95% CI: 0.959 - 1.115). **Curveball (E-H)** Fitness estimation from growth curves of  $2n+1$  and  $2n^*$  at  $39^{\circ}\text{C}$ .  $w_{2n^*}/w_{2n+1}=1.033$  (95% CI: 1.027 - 1.041). Growth curves previously described in Yona et al.<sup>62</sup>, Figs. 3C, 4A, and S2. Fitness estimated from growth curves using Curveball, a method for predicting results of competition experiments from growth curve data<sup>38</sup> [curveball.yoavram.com](http://curveball.yoavram.com). See *Models and Methods, Prior distributions* for more details. **(A,B;E,F)** Mono-culture growth curve data (markers) and best-fit growth models (lines). **(C,G)** The mixed-culture prediction for the strains from A,B and E,F respectively, 6,375 generated curves. **(D,H)** The relative fitness distribution for  $2n+1$  relative to  $2n$  (panel D) and  $2n^*$  relative to  $2n+1$  (panel H). Figures generated by Curveball.

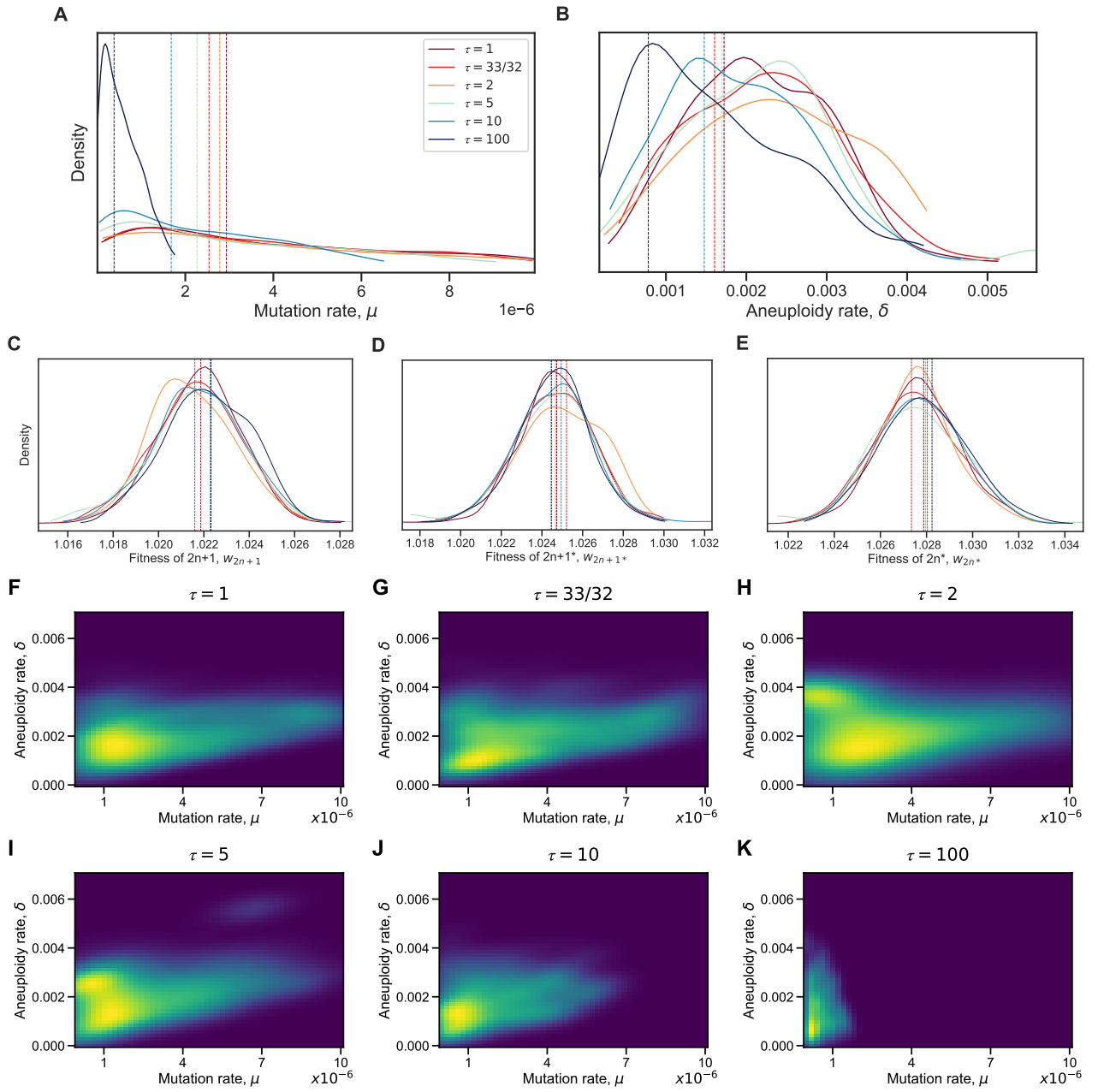


**Figure S4: Model with elevated mutation rate in aneuploid cells.** (A-E) The inferred posterior distributions for models with different values of  $\tau$ , the fold-increase in mutation rate in aneuploid cells ( $2n+1$  and  $2n+1^*$ ). Vertical dashed lines represent the MAP (maximum a posteriori) of each distribution. When the increase in mutation rate is high,  $\tau = 10$  and  $\tau = 100$ , the inferred mutation (A) and aneuploidy (B) rates tend to be lower. (F-K) The inferred joint posterior distribution of mutation rate ( $\mu$ ) and aneuploidy rate ( $\delta$ ) with different  $\tau$  values (dark purple and bright yellow for low and high density, respectively).

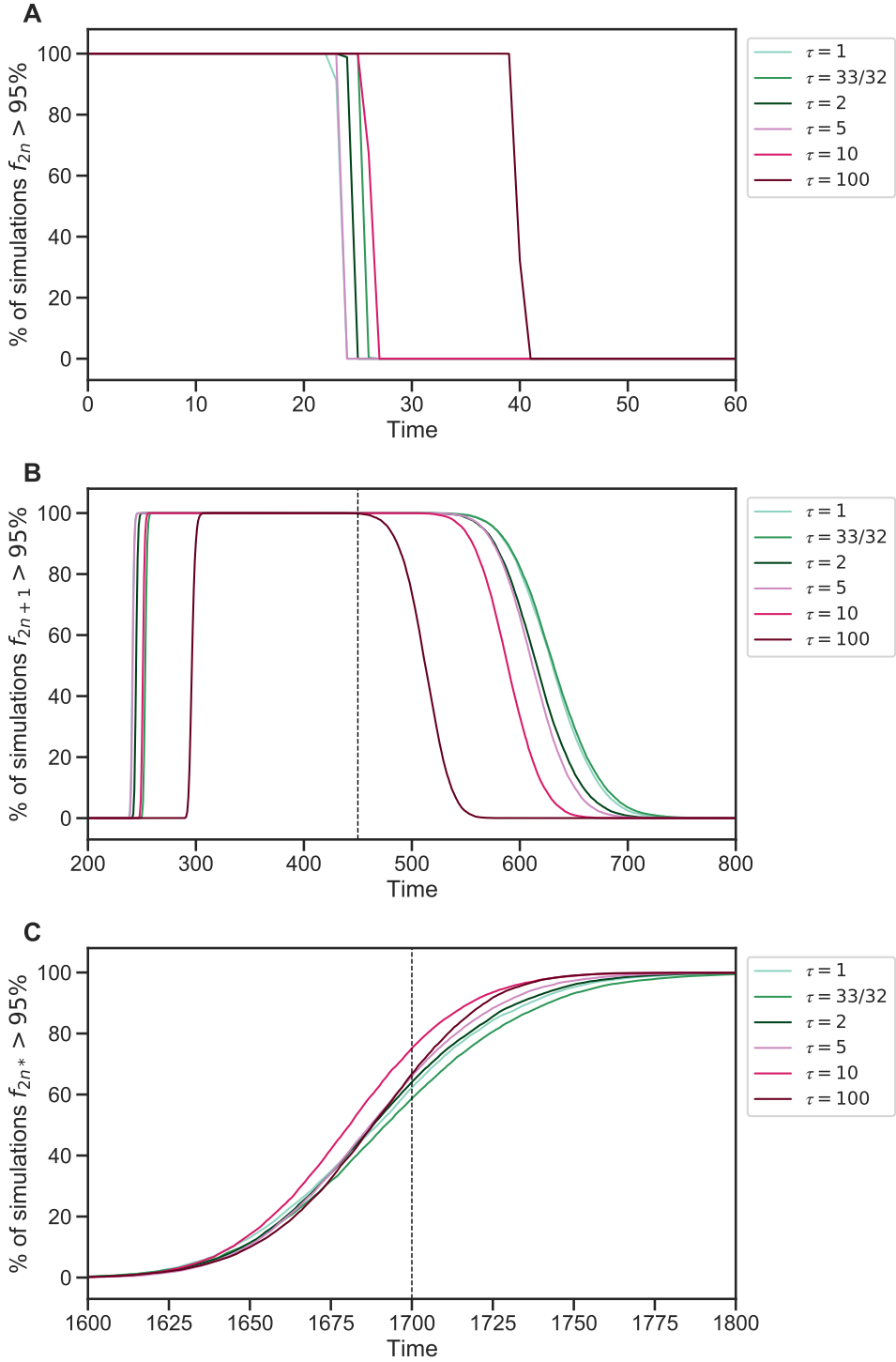


**Figure S5: Genotype fixations for models with increased genetic instability.** We estimated the parameters for different models, each assuming a different value of  $\tau$ , the fold-increase in mutation rate in aneuploid cells. We then generated 10,000 simulations using the MAP estimate of each model and evaluated the fraction of simulations in which the frequency of genotype  $2n$  (**A**),  $2n+1$  (**B**), and  $2n^*$  (**C**) is above 95% (y-axis) at each generation (x-axis). Note that  $2n+1^*$  did not fix. We can see that  $\tau = 100$  can be distinguished if the waiting time for  $f_{2n} < 95\%$  is known (panel A) or if the waiting time for  $f_{2n+1} > 95\%$  or  $f_{2n+1} < 95\%$  is known (panel B). It is harder to distinguish between  $1 \leq \tau \leq 10$ .

**Table S1: Mutant alleles in population  $H2$ .**

Mutant alleles identified in the ancestor (generation 0), aneuploid (generation 450), and evolved (generation 2,350) of population  $H2$ . See supplementary file.

**Table S2: Mutant alleles in population  $H4$ .**

Mutant alleles identified in the ancestor (generation 0), aneuploid (generation 450), and evolved (generation 1,700) of population  $H4$ . See supplementary file.

**Table S3: WAIC values for different  $\tau$  values.**

Model	WAIC
$\tau = 1$	-9
$\tau = 33/32$	-9
$\tau = 2$	-8
$\tau = 5$	-12
$\tau = 10$	-9
$\tau = 100$	-12

WAIC defined in eq. (6).

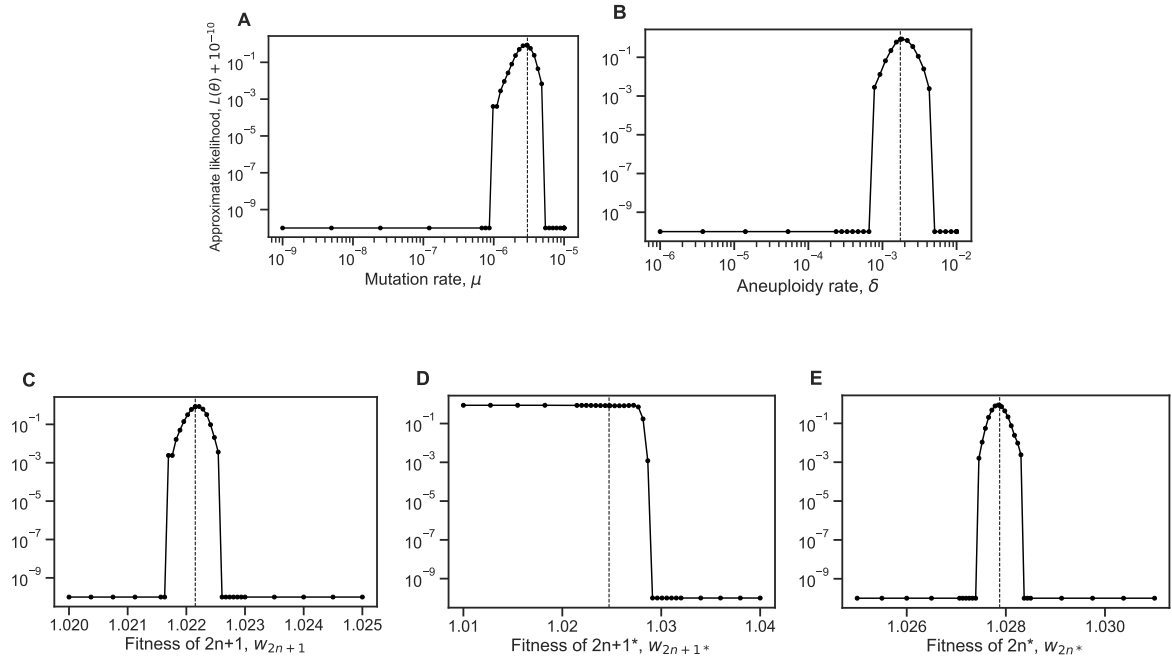


**Figure S6: Likelihood profiles.** Sensitivity of the model approximate likelihood,  $\mathcal{L}(\theta)$ , to changing a single parameter while the other parameters remain fixed at their MAP estimates. Dashed vertical line represents the MAP value. The prior distributions for the mutation rate and aneuploidy rate are  $\mu \sim U(10^{-9}, 10^{-5})$  and  $\delta \sim U(10^{-6}, 10^{-2})$ , respectively.

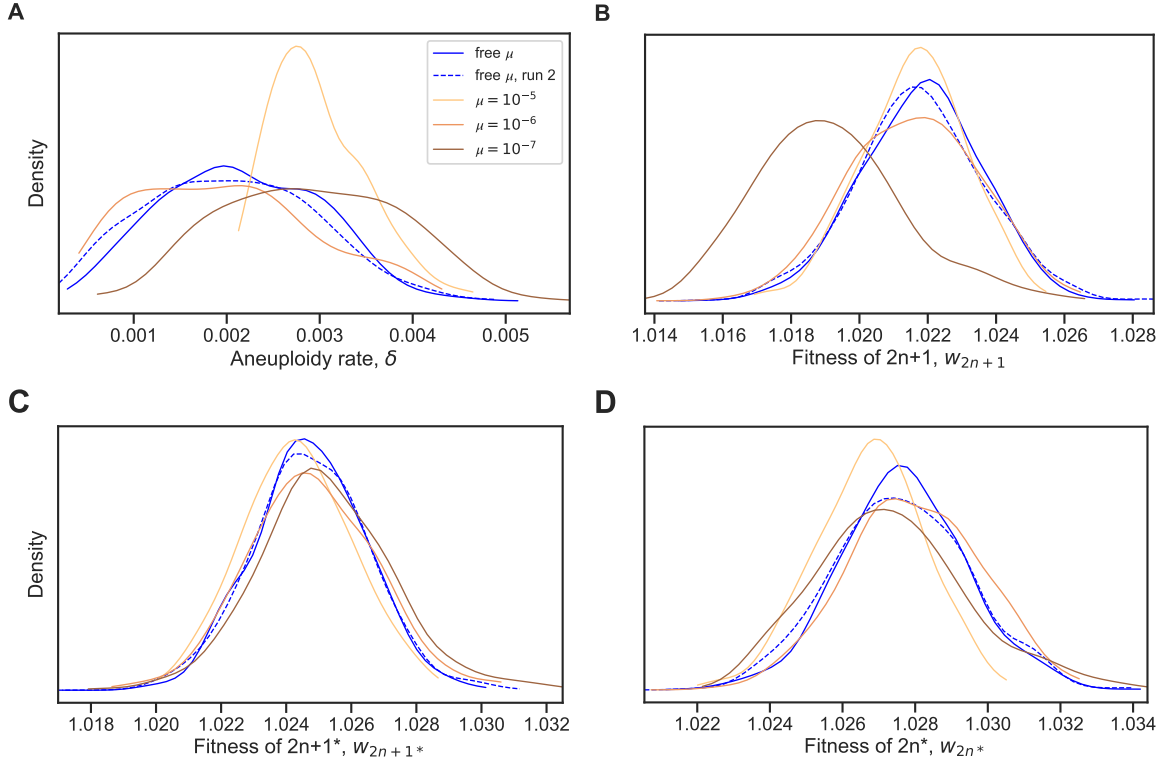


**Figure S7: Model with fixed mutation rate.** (A-D) The inferred posterior distributions for models with free and fixed mutation rate,  $\mu$ . The MAP (maximum a posteriori) and 50% HDI (highest density interval) for each model are: **free  $\mu$ , run 1:**  $\delta = 1.720 \cdot 10^{-3}$  [ $1.470 \cdot 10^{-3} - 2.786 \cdot 10^{-3}$ ],  $w_{2n+1} = 1.022$  [1.021 – 1.023],  $w_{2n+1^*} = 1.025$  [1.024 – 1.026],  $w_{2n^*} = 1.028$  [1.026 – 1.029]; **free  $\mu$ , run 2:**  $\delta = 2.129 \cdot 10^{-3}$  [ $1.334 \cdot 10^{-3} - 2.695 \cdot 10^{-3}$ ],  $w_{2n+1} = 1.022$  [1.02 – 1.023],  $w_{2n+1^*} = 1.025$  [1.023 – 1.026],  $w_{2n^*} = 1.028$  [1.026 – 1.029];  **$\mu = 10^{-5}$ :**  $\delta = 2.903 \cdot 10^{-3}$  [ $2.399 \cdot 10^{-3} - 3.156 \cdot 10^{-3}$ ],  $w_{2n+1} = 1.022$  [1.021 – 1.023],  $w_{2n+1^*} = 1.024$  [1.023 – 1.025],  $w_{2n^*} = 1.027$  [1.026 – 1.028];  **$\mu = 10^{-6}$ :**  $\delta = 1.917 \cdot 10^{-3}$  [ $9.624 \cdot 10^{-4} - 2.447 \cdot 10^{-3}$ ],  $w_{2n+1} = 1.022$  [1.02 – 1.023],  $w_{2n+1^*} = 1.025$  [1.023 – 1.026],  $w_{2n^*} = 1.028$  [1.027 – 1.029];  **$\mu = 10^{-7}$ :**  $\delta = 2.901 \cdot 10^{-3}$  [ $2.139 \cdot 10^{-3} - 3.671 \cdot 10^{-3}$ ],  $w_{2n+1} = 1.019$  [1.017 – 1.02],  $w_{2n+1^*} = 1.025$  [1.024 – 1.026],  $w_{2n^*} = 1.027$  [1.026 – 1.029].

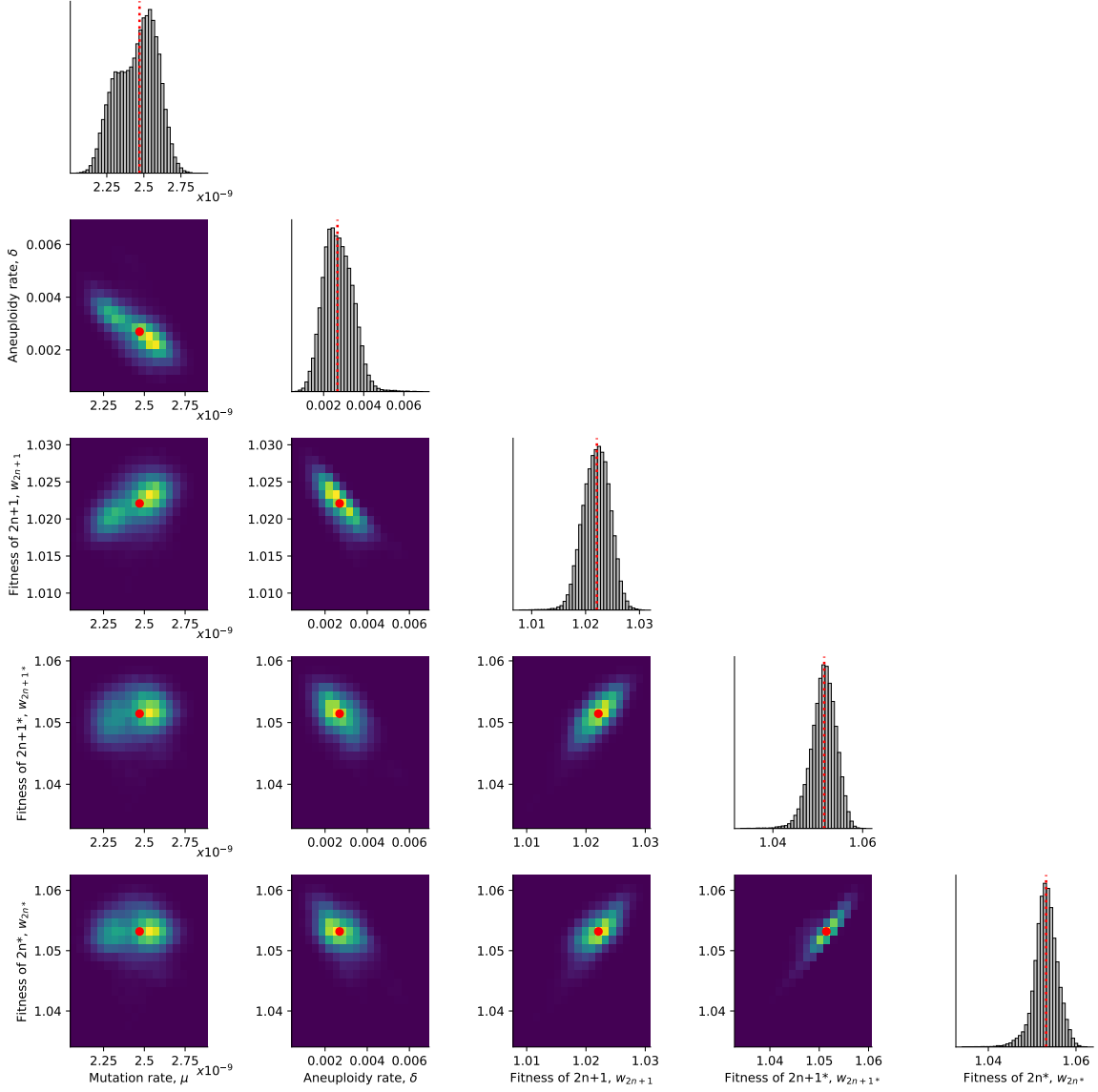


**Figure S8: Posterior distribution of parameters inferred with the extended prior distribution.** On the diagonal, the inferred posterior distribution of each model parameter. Below the diagonal, the inferred joint posterior distribution of pairs of model parameters (dark purple and bright yellow for low and high density, respectively). Red markers and orange lines for the joint MAP estimate (which may differ from the marginal MAP, as the marginal distribution integrates over all other parameters).

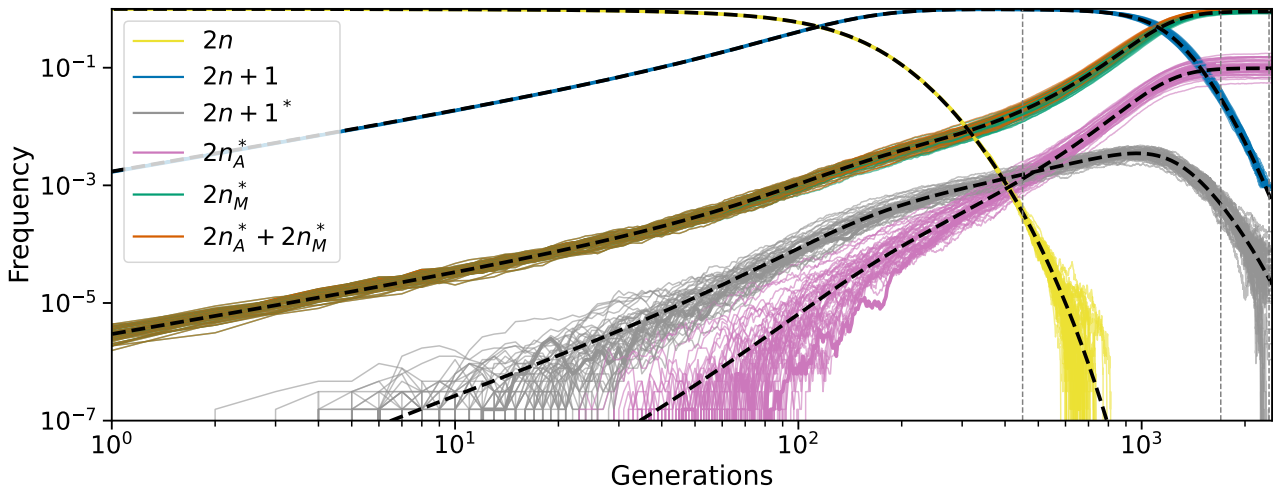


**Figure S9: Posterior predicted genotype frequencies in log-log scale.** Frequency dynamics of the different genotypes with MAP parameter estimates, same as Figure 5A, but in log-log scale. Black dashed curves for a deterministic model without genetic drift. Clearly, appearance of  $2n+1$  and  $2n_M^*$  is deterministic. Appearance of  $2n+1^*$ , and therefore  $2n_A^*$ , is stochastic, however, the frequency dynamics are deterministic above a frequency of roughly 0.001. Note that the  $2n_M^*$  and the  $2n_A^* + 2n_M^*$  lines are overlapping for much of their trajectories.

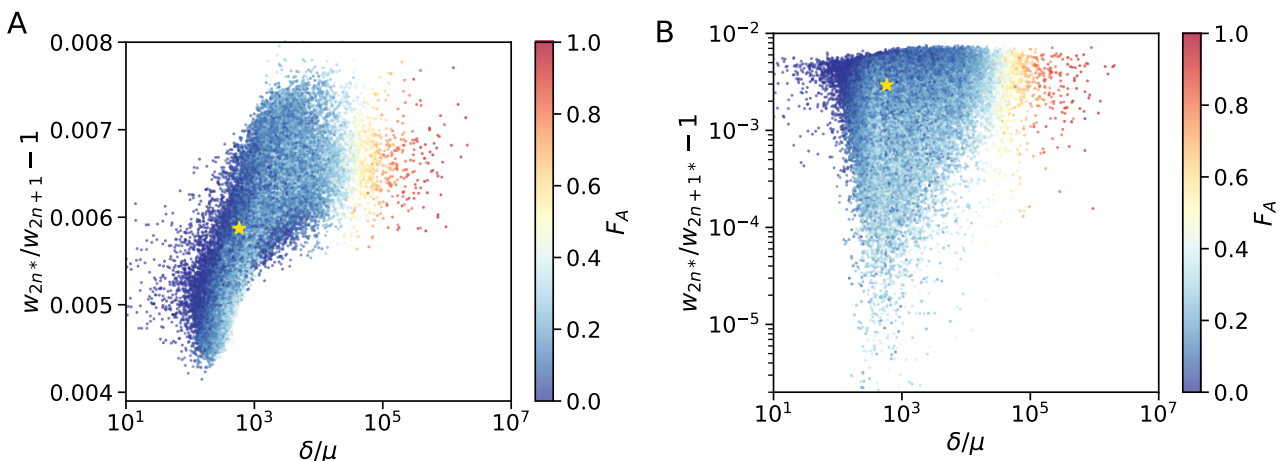


**Figure S10: Posterior distribution of  $F_A$ .** (A,B)  $F_A$  values (color coded) as in Figure 5 for different parameter choices on the x- and y-axes. White star denotes the MAP estimate.